Adhesion Characteristics and Swelling Response of Stimuli-Responsive Hydrogels

by
Chandler Benjamin

A dissertation submitted in partial fulfillment
of the requirements for the degree of

Doctor of Philosophy
(Engineering Mechanics)

at the

UNIVERSITY OF WISCONSIN-MADISON
2017

Date of final oral examination: 7/24/2017

The dissertation is approved by the following members of the Final Oral Committee:

Wendy Crone, Professor, Engineering Physics
Roderic Lakes, Professor, Engineering Physics
Lih-Sheng Turng, Professor, Mechanical Engineering
Susan Coppersmith, Professor, Physics
Robert Witt, Associate Professor, Engineering Physics

Abstract

Stimuli-responsive hydrogels are a class of shape memory materials that have been successfully used in microfluidic and biomedical devices and additionally as biomaterials. These materials operate in a hydrated environment and respond with a significant volumetric reversible transformation through absorption or release of water within the polymeric network. The pH sensitive 2-hydroxyethyl methacrylate (2 - dimethylamino) ethyl methacrylate, (HEMA-DMAEMA) stimuli-responsive hydrogel is used in microfluidic devices as sensors and actuators. This hydrogel responds to an acidic aqueous environment with a subsequent volume change. This actuation requires the hydrogel to be in an acidic environment to remain in its swollen state.

In chapter 2 I initially characterize this hydrogel in terms of engineering properties such as the storage modulus G', the loss modulus G'' and loss tangent $\tan(\delta)$. The storage modulus is analogous to the shear modulus from elasticity theory. The loss modulus is a representation of energy dissipation from applied loading. The loss tangent $\tan(\delta)$ is a measure of damping in a material.

In chapter 3 I develop a method of measuring the Fung parameter β° for stimuli-responsive hydrogels using a simple tensile test. HEMA-DMAEMA stimuli-responsive hydrogels are examined using this method. The HEMA-DMAEMA is pre-conditioned in 3.0 (acidic) pH and 11.0 (basic) pH buffer solutions prior to testing to compare the theoretical results to experiment in both the swollen and unswollen states. The measured Fung parameter β° is 0.870 ± 0.018.

In chapter 4 I examine the interfacial adhesion of HEMA-DMAEMA. Experimental observations have given indications that the adhesion of the (HEMA-DMAEMA) is effected by substrate modifications. Using a unique experimental technique coupled with concepts from fracture mechanics I measure differences in the adhesive strength of HEMA-DMAEMA on borosilicate glass substrates, both unmodified and with different surface modifications.

Together these hydrogel characteristics provide microfluidic device designers the ability to plan their designs around viscoelastic effects such as creep, relaxation, and interfacial phenomena such as adhesion.

Acknowledgements

I want to thank my advisor, Professor Wendy C. Crone for giving me the opportunity of being part of her research group and the chance to pursue my dream of obtaining a Ph.D. She made the entire journey through graduate school an enjoyable and unforgettable experience.

I am grateful to my thesis committee members Professor Roderic Lakes, Professor Lih-Sheng Turng, Professor Susan Coppersmith and Professor Robert Witt for agreeing to guide me back to the right course of action through my many missteps.

I would like to thank the many professors that I have taken courses with and have guided me with their exceptional scientific knowledge. I would especially like to mention Professor Roderic Lakes and Professor Walter Drugan for they provided me with my foundation in solid mechanics.

I want to recognize my current and former lab members, Brett Napawocki, Alana Stempien, Suehelay Acevado-Acevedo (former), Max Salick (graduated).

I would also like to acknowledge the many valuable conversations I have had over the years with Dr. Mehrdad Arjmand about mechanics of materials and life in general.

I would also like the thank the past and current undergraduate students John C. Springmann, Shahzad Chindhy and Rachel Craven for their invaluable assistant in performing experiments that lead to many of the procedural changes that took place over the many years of experiments.

I would additionally like to acknowledge all of my brothers and sister and both of my parents may they rest in peace for never giving up on me.

A special thanks goes to Suehelay Acevado-Acevado. We both started graduate school at the same time and shared a cubicle. She has been my very best friend for the past six years and I cannot imagine what this journey would have been like without her.

Finally I would like to acknowledge my partner Heidi L. Turner for without her constant love and support this journey of mine would not have been possible.

Contents

List of Figures

List of Tables

List of Mathematical Symbols

$s_{\theta z}$	Deviatoric stress
G'	Storage Modulus
G"	Loss Modulus
$\epsilon_{\theta z}$	Deviatoric strain
$\dot{\epsilon}_{\theta z}$	Deviatoric strain rate
$\tan(\delta)$	Measure of damping
$\mathbf{S}$	2nd Piola-Kirchoff stress tensor
λ	Stretch
β°	Fung parameter
$\mathbf{E}$	Green strain tensor
G	Shear modulus

$W(\mathbf{E}, \mathbf{S}; \mathbf{C})$	Implicit strain energy function, Lagrangian
$\mathbf{M}$	Tangent modulus
$W(\mathbf{E})$	Explicit strain energy function
$\mathbf{J_c}$	Implicit compliance tensor
$\mathscr{G}$	Strain energy release rate
$\mathscr{R}$	Crack resistance
$\mathscr{W}$	Strain energy density function
$\mathbf{\Pi}$	Extra stress
$\mathbf{C}$	Green deformation tensor
E_a	Apparent modulus

This thesis is dedicated to my mother and father.

May they rest in peace...

Chapter 1

Introduction

1.1 Stimuli Responsive Hydrogels

Smart stimuli-responsive hydrogels are used in microfluidic devices such as sensors and actuators. These soft materials can undergo large volume changes when introduced to an external stimulus. A device designer in the field of microfluidics needs to have a sound fundamental understanding of the material properties of these gels, otherwise they cannot design a structure efficiently. Currently device designers need to rely heavily on trial and error to optimize their designs. There is a lack of understanding of these material's basic mechanical properties.

The material studied in this thesis, (2 - hydroxyethyl methacrylate) (HEMA) 2 - (dimethylamino) ethyl methacrylate (DMAEMA) stimuli responsive hydrogels, are a polymeric material that displays some amazing characteristics when exposed to certain external

stimulus. Specifically for HEMA-DMAEMA that stimulus is an external buffer solution of an acidic pH. If the conditions are right the material will expand beyond original volume and returns to its original volume once the stimulus is removed, thus displaying the shape memory effect. This same material will always come back to its original size, shape and dimensions if the external stimulus is removed.

1.2 Shape Memory Materials

The study of shape memory materials spans many different disciplines and demands a fundamental knowledge of chemistry, physics and engineering. The mechanics of the interaction of a responsive hydrogel to its surroundings is important in the fields of microfluidics and microelectromechanical-based devices (MEMS). In these areas of engineering, the ability to fabricate responsive hydrogels into various complicated geometries garnered these hydrogels much deserved interest.

Hydrogels share a unique characteristic with solids in that they do not flow. On the other hand they also share the unique characteristic of fluids in that they allow small molecules to diffuse into them. At their core a hydrogel is a three-dimensional, cross-linked, network of hydrophilic polymer chains that form homopolymers or copolymers. The chemical cross-linking through covalent bonding is stable, whereas the physical cross-linking interactions (such as hydrogen-bonding, ionic bonding, van der Waals forces, dipole-dipole interactions, etc.) are susceptible to environmental changes and their disruption can lead to structural transformation, i.e. swelling-shrinking transitions. Examples of chemical

hydrogels are contact lenses and the absorbent baby diapers. An example of a common physical hydrogel is jello. [5, 13, 16].

While there are many different hydrogels the three most common gels used for engineering purposes are poly(vinyl alcohol) (PVA), poly (2 - hydroxyethyl methacrylate) (PHEMA), and poly(ehtylene oxide) (PEO).

PHEMA hydrogels can be prepared via bulk copolymerization of monomers with a cross-linking agent, cross-linking of polymers in solution and simultaneous copolymerization and cross-linking of a monomer with a cross-linking agent in solution. Simultaneous copolymerization and cross-linking is one method that is used commonly because of the speed of polymerization and a desired shape for the polymerization of the gel can be obtained easily because the polymer starts in liquid form[15, 17]. PHEMA gels are normally prepared via free radical polymerization. The cross linking agents most commonly used are ethylene glycol dimethacrylate (EGDMA), diethylene glycol dimethacrylate (DEGDMA) and tetraethylene glycol (TEGDMA)[6].

PHEMA hydrogels have been shown to be strong mechanically. Additionally they are chemically stable. These two properties have garnered them much attention in the field of biomedicine. Swelling properties of PHEMA have been studied extensively[11, 24] and often the solution used to swell the hydrogel differs from the solution used to prepare it. It is not uncommon for the hydrogel to reach three times its original volume based on the comonomer it is polymerized with.

PHEMA hydrogels possess a cross-linked structure. This allows them to behave much like a solid but retain its characteristic 95% to 99% ratio of water to solid.

In 1980 Tanaka et.al.[20] observed the equilibrium phase transition of ionic gels. From this observation the intense study of stimuli-responsive gels was born. For stimuli-responsive hydrogels, depending on the functional groups that reside along the polymer chain, various stimuli can cause a response within the hydrogel, dictating how much water the hydrogel absorbs or releases[2, 3, 14, 26].

pH-Sensitive hydrogels, undergo a volume transition from when introduced to an appropriate external buffer solution[1, 4, 7]. These responsive hydrogels have ionizable functional groups on their polymer chains that have pH-sensitivity. The main components of pH-sensitive hydrogels are a pH-sensitive monomer that controls the hydrogels phase transition and an inert monomer that controls the mechanical properties. For hydrogels that expand in basic solutions a common pH-sensitive monomer is acrylic acid (AA)[9]. For hydrogels that expand in acidic solution a common pH-sensitive monomer is 2-(dimethylamino)ethyl methacrylate (DMAEMA)[19, 22]. One of the most common inert monomer used in pH-sensitive hydrogel fabrication is 2-hydroxyethyl methacrylate (HEMA). A feature of these hydrogels is a *critical pH* that is the volume transition pH of the gel. The chemistry of the hydrogels composition can be adjusted to change the critical pH of the gel[26].

Temperature-sensitive hydrogels, undergo a volume transition when a change in local

environmental temperature occurs[2, 18]. A very commonly used monomer is N - isopropylacrylaminde (NIPAAm)[23]. These temperature-sensitive polymers have a point known as the *lower critical solution temperature* (LCST) which is the common temperature at which a phase transition occurs. The LCST can be adjusted by adjusting the composition of the polymer as well[8, 23, 26]

Electro-responsive hydrogels, undergo a volume transition or undergo bending when exposed to an external electric field[10, 12, 21, 25]. In 1982 Tanaka, et.al,[21] demonstrated that by changing the external electrical field surrounding a hydrogel a reversible volume transition occurred. This was one of the first examples of a stimuli-responsive hydrogel. One common feature of these hydrogels is that they often are also responsive to temperature or pH environmental changes.

The field of microfluidics has a long and rich history but the widespread application of responsive hydrogels in microfluidics devices is relatively new. The physics of these materials varies greatly as size scale is reduced. Much of the device design in this area is trial and error and basic engineering parameters are unknown. Results in the basic physics of these responsive hydrogels used on this size scale is lacking and is a wide open area for exploration. This thesis seeks to explore the basic physical properties of HEMA-DMAEMA stimuli-responsive hydrogels which has applications to their use in microfluidic devices as sensors and actuators.

Bibliography

[1] David J Beebe, Jeffrey S Moore, Joseph M Bauer, Qing Yu, Robin H Liu, Chelladurai Devadoss, and Byung-Ho Jo. Functional hydrogel structures for autonomous flow control inside microfluidic channels. *Nature*, 404(6778):588–590, 2000.

[2] S. Cai and Z. Suo. Mechanics and chemical thermodynamics of phase transition in temperature-sensitive hydrogels. *Journal of the Mechanics and Physics of Solids*, 59(11):2259 – 2278, 2011. ISSN 0022-5096. doi: 10.1016/j.jmps.2011.08.008. URL http://www.sciencedirect.com/science/article/pii/S0022509611001670.

[3] Sudipto K De, NR Aluru, B Johnson, WC Crone, David J Beebe, and J Moore. Equilibrium swelling and kinetics of ph-responsive hydrogels: Models, experiments, and simulations. *Microelectromechanical Systems, Journal of*, 11(5):544–555, 2002.

[4] David T Eddington and David J Beebe. Flow control with hydrogels. *Advanced drug delivery reviews*, 56(2):199–210, 2004.

[5] Paul J. Flory. *Principles of polymer chemistry*. Cornell University Press, 1953.

[6] DONALD E GREGONIS, CHWEN M CHEN, and JOSEPH D ANDRADE. The chemistry of some selected methacrylate hydrogels. ACS Publications, 1976.

[7] B.D Johnson, D.J Beebe, and W.C Crone. Effects of swelling on the mechanical properties of a ph-sensitive hydrogel for use in microfluidic devices. *Materials Science and Engineering: C*, 24(4):575 – 581, 2004. ISSN 0928-4931. doi: 10.1016/j.msec.2003.11.002. URL http://www.sciencedirect.com/science/article/pii/S0928493103002947.

[8] Hideya Kawasaki, Shigeo Sasaki, Hiroshi Maeda, and Katsuyoshi Nishinari. Effect of the introduced charge on the thermal behavior of n-isopropylacrylamide gels in water and nacl solutions. *Langmuir*, 16(7):3195–3199, 2000.

[9] Jungsoo Kim and David A Tirrell. Synthesis of well-defined poly (2-ethylacrylic acid). *Macromolecules*, 32(3):945–948, 1999.

[10] Yong Li and Toyoichi Tanaka. Kinetics of swelling and shrinking of gels. *The Journal of chemical physics*, 92:1365, 1990.

[11] Jean-Pierre Montheard, Michel Chatzopoulos, and Daniel Chappard. 2-hydroxyethyl methacrylate (hema): chemical properties and applications in biomedical fields. *Journal of Macromolecular Science, Part C: Polymer Reviews*, 32(1):1–34, 1992.

[12] Y. Osada and J.P. Gong. Soft and wet materials: polymer gels. *Advanced Materials*, 10:827–837, 1998.

[13] GA Paleos. What are hydrogels? *Pittsburgj Plastic Manufacturing, Butler, PA*, 2012.

[14] Nikolaos A Peppas. Physiologically responsive hydrogels. *Journal of bioactive and compatible polymers*, 6(3):241–246, 1991.

[15] Nikolaos A Peppas, Humphrey J Moynihan, and Lucy M Lucht. The structure of highly crosslinked poly (2-hydroxyethyl methacrylate) hydrogels. *Journal of biomedical materials research*, 19(4):397–411, 1985.

[16] Nikolaos A Peppas et al. *Hydrogels in medicine and pharmacy*, volume 3. CRC press Boca Raton, FL, 1987.

[17] MF Refojo and H Yasuda. Hydrogels from 2-hydroxyethyl methacrylate and propylene glycol monoacrylate. *Journal of Applied Polymer Science*, 9(7):2425–2435, 1965.

[18] H. Shirota, N. Endo, and K. Horie. Volume phase transition of polymer gel in water and heavy water. *Chemical Physics*, 238(3):487 – 494, 1998. ISSN 0301-0104. doi: 10.1016/S0301-0104(98)00340-1. URL http://www.sciencedirect.com/science/article/pii/S0301010498003401.

[19] Ronald A Siegel and Bruce A Firestone. ph-dependent equilibrium swelling properties of hydrophobic polyelectrolyte copolymer gels. *Macromolecules*, 21(11):3254–3259, 1988.

[20] Toyoichi Tanaka, David Fillmore, Shao-Tang Sun, Izumi Nishio, Gerald Swislow, and Arati Shah. Phase transitions in ionic gels. *Physical Review Letters*, 45(20):1636, 1980.

[21] Toyoichi Tanaka, Izumi Nishio, Shao-Tang Sun, and Shizue Ueno-Nishio. Collapse of gels in an electric field. *Science*, 218(4571):467–469, 1982.

[22] P Van de Wetering, NJ Zuidam, MJ Van Steenbergen, OAGJ Van der Houwen, WJM Underberg, and WE Hennink. A mechanistic study of the hydrolytic stability of poly (2-(dimethylamino) ethyl methacrylate). *Macromolecules*, 31(23):8063–8068, 1998.

[23] Heiko van der Linden, Wouter Olthuis, and Piet Bergveld. An efficient method for the fabrication of temperature-sensitive hydrogel microactuators. *Lab on a Chip*, 4(6):619–624, 2004.

[24] O Wichterle and R Chromeček. Polymerization of ethylene glycol monomethacrylate in the presence of solvents. In *Journal of Polymer Science: Polymer Symposia*, volume 16, pages 4677–4686. Wiley Online Library, 1967.

[25] Yajiang Yang and Jan BFN Engberts. Stimuli response of polysoap hydrogels in aqueous solution and dc electric fields. *Colloids and Surfaces A: Physicochemical and Engineering Aspects*, 169(1):85–94, 2000.

[26] Qing Yu. *Development of functional polymeric materials for microfluidic systems*. PhD thesis, University of Illinois at Urbana-Champaign, 2002.

Chapter 2

Viscoelastic Properties of HEMA-DMAEMA

2.1 Dynamic Testing

2.2 Introduction

Most real materials have the capacity to store and dissipate mechanical energy. An elastic solid can store mechanical energy with no dissipation while a newtonian viscous fluid can dissipate energy but cannot store energy. These two descriptions are ideal states of matter that are seldom realized in real materials. Most real materials, to varying degrees, can store and dissipate mechanical energy. These materials are categorized as viscoelastic[15, 26].

The pH sensitive 2-hydroxyethyl methacrylate (2 - dimethylamino) ethyl methacrylate, (HEMA-DMAEMA) stimuli-responsive hydrogel, is a viscoelastic polymer that displays dramatic changes in mechanical properties based on different external conditions. The ability of this material to increase volume when exposed to an acidic external buffer solution naturally gives the polymer use as sensors[23] or actuators[19] in microfluidic devices. The response times of these materials are very slow, they have low stiffness and low ultimate tensile strength and would be a poor component material on the macro scale. When dimensions become small enough (milli-micro meter) the response times for volumetric expansion change from hours to minutes and these hydrogels become excellent active materials for use in microfluidic devices[3]. Active stimuli-responsive hydrogels have also been used in genomics[13, 21, 29] proteomics[5, 12, 17] and metabolomics[14, 31] as components.

An understanding of chemical and mechanical properties of hydrogels is required in the design of hydrogel hybrid systems, nanostructures, and hybrid polymers [20, 22]. Autonomous microfluidics have been developed with the aid of stimuli-responsive hydrogels[5] where research into adaptive microlens[6], variable focus lens[7], and light sensitive hydrogels for nano-composites[18] have been advanced. Additionally in cellular and tissue engineering, temperature responsive hydrogels have been used to regulate cell morphology[30]. Stimuli-responsive hydrogels have also seen many uses in different emerging areas of biological research[2, 9, 25].

Prior studies of other active stimuli-responsive polymers have consisted of creep, relaxation, and stress or strain sweeps conducted at 3 pH and 7 pH buffer solutions. These

tests were conducted to determine the suitability of using a DMAEMA based responsive hydrogel in controlled drug delivery and tissue engineering applications[28]. Additionally the non-linear behavior of the PMMA-PDMAEMA-PMMA was studied at 3.5 pH where creep behavior was reported for five strain levels showing non-linear strain dependent relaxation behavior[4]. The monomer 2-hydroxyethyl methacrylate (HEMA) is combined with monomers Acrylic Acid (AA) or (2 - dimethylamino) ethyl methacrylate (DMAEMA) to form a pH responsive copolymer hydrogel. The HEMA-AA copolymer is responsive to basic solutions and the (HEMA-DMAEMA) copolymer is responsive to acid solutions[11]. These two pH sensitive hydrogels are used in microfluidic applications as actuators and sensors for adjustable lens[16], micropumps and micromixers[1] and piezoresistive sensors[10]. HEMA-AA swells in basic solution and HEMA-DMAEMA swelling in an acidic solution. Actuators and sensors in these devices need to have certain properties to be successfully implemented. The sensor needs a 'sensing' mechanism in that can be tuned for particular applications and an actuator needs to be controllable and repeatable. The advantage that stimuli-responsive hydrogels have in microfluidic devices is that they possess both a sensing and actuation mechanism in one structural material. HEMA-DMAEMA stimuli-responsive hydrogels can 'sense' an acidic external buffer solution and it can 'actuate' by changing volume in response the acidic buffer. Understanding the mechanical response of these hydrogels in an acidic (3.0 pH) and basic (11.0 pH) environment is essential to device design.

The purpose of this paper to characterize the mechanical properties of HEMA-DMAEMA stimuli-responsive hydrogels in these two environments in terms of engineering properties

such as the storage G' and loss G'' modulus and $\tan(\delta)$. The creep response of these materials is also investigated and the non-linear aspects of the hydrogel studied in the separate swelling conditions is observed.

2.3 Sample Preparation

A prepolymer solution is prepared using the reagents, 2-(dimethylamino) ethyl methacrylate (DMAEMA), 2-hydroxyethl methacrylate (HEMA), ethylene glycol dimethacrylate (EGDMA) and 2,2-dimethoxy-2-phenylacetophenone (DMPA). The reagents are mixed together in the following ratios, 25.77:5.718:0.467:1. All reagents were purchased from Sigma-Aldrich. Prior to polymerization this hydrogel-liquid solution is stored at $-8°$C.

2.4 Shear Rheometry

Samples are fabricated into cylindrical wafers 12.5 mm in radius and 0.5 to 1.0 mm in height. As depicted in figure 2.1 a flat PDMS slab of thickness 1.0 mm was fabricated. A circular well is cut out of the Polydimethylsiloxane (PDMS) slab that is 15 mm in radius. The slab is then cut down to the size of a standard petri dish. A glass cover slip is placed down first into the petri dish, then the PDMS mold is secured on top of the glass cover slip. The pre-polymer solution is then poured into the well. Once this is done another glass cover slip is placed on top of the PDMS mold. A photo-resistant circular pattern is placed on top of the glass cover slip. The circular pattern has a radius of 12.5

mm. The assembly is then exposed to ultra-violet light at an intensity of 20 mW/cm^2 for a total of 120 seconds. The circular sample is then formed and removed from the mold. The sample is then swollen in 11.0 pH buffer solution for a total of 48 hours prior to testing and tested immediately upon removal from the buffer to maintain a hydrated state throughout the testing.

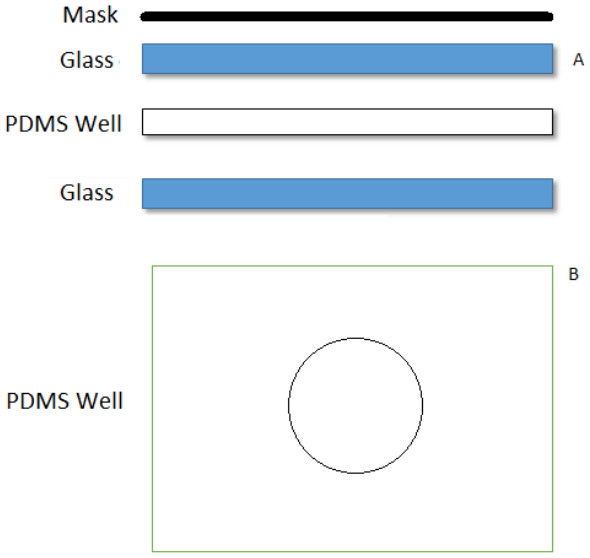

FIGURE 2.1: Schemactic of the assembly used for fabrication of HEMA-DMAEMA samples. A.) A glass cover slip is placed on the bottom and top of the PDMS mold. In B.) A top-down view of the PDMS mold with circular well in the center for the pre-polymer solution is located.

A TA Instruments model AR 2000 ex DHR-1 rheometer with a parallel plate attachment is used to determine the dynamic moduli and the relaxation modulus in shear. The parallel plate rheometer measures normal force, torque and radial displacement.

The torque (T) is recorded by the rheometer during testing and the shear stress is given via, $s_{\theta z}(R) = 2T/\pi R^3$. It should be noted that for a parallel plate rheometer the stress, $s_{\theta z}$, does vary as a function of radius and the machine measure the torque at the outer

most point of the plate. This is important because the sample being tested needs to be as large as the parallel plate and no smaller. Otherwise the machine gives erroneous results. The storage G' and loss G'' can be determined via,

$$s_{\theta z}(t) = \epsilon^o_{\theta z}(G'(\omega)sin(\omega t) + G''(\omega)cos(\omega t)) \tag{2.1}$$

where $\epsilon_{\theta z}$ is the pre-determined shear strain amplitude. The maximum shear strain is determined by $\epsilon_{\theta z} = R\theta/H$ where R is the outer radius of the sample, H is the height, or thickness of the sample and θ is the angular displacement. The shear strain rate is determined via, $\dot{\epsilon}_{\theta z}(t) = R\Omega/H$, where Ω is the calculated angular velocity. For a sinusoidal input of $\epsilon_{\theta z}(t) = \epsilon^o_{\theta z}sin(\omega t)$ the shear rate is $\dot{\epsilon}_{\theta z}(t) = \epsilon^o_{\theta z}\omega cos(\omega t)$. From these relationships equation (2.1) can be rewritten as,

$$s_{\theta z}(t) = G'\epsilon_{\theta z}(t) + G''\frac{\dot{\epsilon}_{\theta z}}{\omega}, \tag{2.2}$$

where $s_{\theta z}(t)$, $\epsilon_{\theta z}$, $\dot{\epsilon}_{\theta z}$ and ω are determined experimentally.

The shear rate is determined based on the known value for the outer radius R, the height of the sample H and the measured angular velocity Ω via, $\dot{\gamma}_r = R\Omega/H$. To determine the dynamic moduli a sinusoidally varying strain of 1% is applied in shear for a frequency range of 0.1 Hz to 100 Hz. The maximum frequency of the parallel plate rheometer used is 100 Hz. For shear relaxation a shear strain as applied with a rise time 0.02 seconds. The shear stress is calculated based on the measured torque T and the known value for

the outer radius R via the formula, $\tau_R = \frac{3T}{2\pi R^3}$. The relaxation is recorded over three decades of time from 0.1 to 100 seconds. For testing 6 samples were prepared and each sample was tested 3 times for a total of eighteen trials (n=18) at each pH value (3.0 pH and 11.0 pH). Each dynamic test was taken over a 0.1 Hz to 100 Hz frequency range with ten data points recorded for each decade at 1% strain. The samples were fabricated and pre-swollen first in 11.0 pH buffer solution for a period of 48 hours before testing. Once the data was recorded the same samples were then immersed in 3.0 pH buffer solution and allowed to swell for a period of 48 hours prior to testing. When mounted in the rheometer samples were compressed until the normal load was at 15.0 N or higher, which amounted to 2%-3% strain, to ensure no slippage when recording data. For dynamic testing data is plotted on a log-log scale over the 0.1 Hz to 100 Hz frequency range for G', G'', and $tan(\delta)$. The error bars given in the reported data are the standard deviations for all experiments run, (n=18) for 3.0 pH and 11.0 pH. For creep n = 3 for each stress level tested. The tests were run from 1 seconds out to 1000 seconds.

2.5 Results

For the experiments reported below pH-sensitive 2-hydroxyethyl methacrylate (2-dimethylamino) ethyl methacrylate (HEMA-DMAEMA) hydrogels is tested in shear using a TA instruments DHR-1 load controlled rheometer with a parallel plate attachment.

Figure 2.2 displays the storage G' and loss G'' modulus as a function of frequency. The frequency range tested is between 0.1 Hz and 100 Hz. For the samples swollen in 3.0

pH buffer solution the hydrogel has a small loss modulus and displays minimal frequency dependence over the range tested. The hydrogel pre-conditioned in 11.0 pH are stiffer in comparison to the samples pre-conditioned in 3.0 pH buffer solution. The frequency dependence of the storage and loss modulus is shown clearly for samples swollen in 11.0 pH solution. A total of 15 samples were tested for the 3.0 pH pre-condition and 17 samples were tested for the 11.0 pH pre-condition.

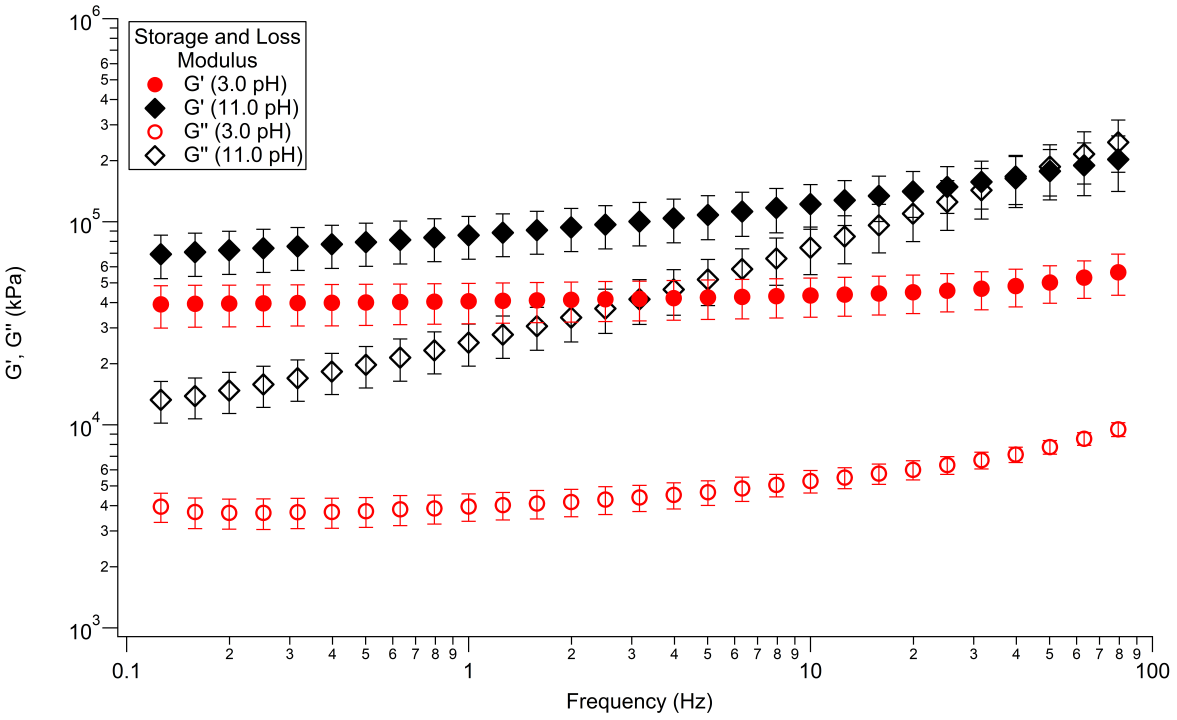

FIGURE 2.2: A comparison of the storage and loss moduli for samples pre-conditioned in 3.0 pH and 11.0 pH buffer solutions.

Figure 2.3 shows a comparison of $\tan(\delta)$ for the pre-conditions of 3.0 pH and 11.0 pH buffer solutions. For samples conditioned in 3.0 pH the gel showed little difference in

tan(δ) between the frequency range of 1 Hz and 10 Hz with the value of tan(δ). For samples pre-conditioned in 11.0 pH buffer solution the samples showed moderate frequency dependence.

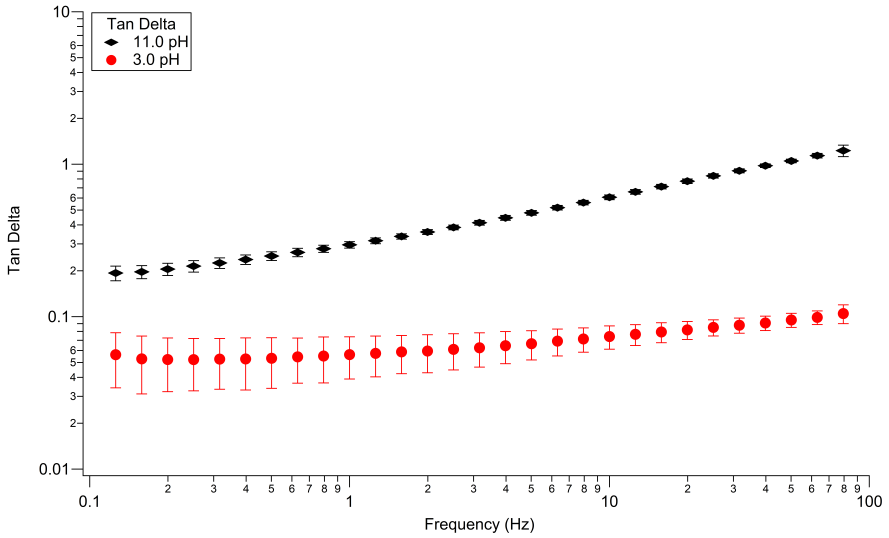

FIGURE 2.3: Tan(δ) for HEMA-DMAEMA pre-swollen in 3.0 (circles) and 11.0 (diamonds) pH buffer solution. Test is conducted on the frequency range of 0.1 Hz to 100 Hz.

Figure 2.4 and 2.5 show the creep compliance for samples swollen in 3.0 pH and 11.0 pH buffer solution respectively. The creep compliance was fit to a power law function, $J(t) = At^n$ with A representing the creep value at 1 second and n representing the creep strength. Samples tested in the 3.0 pH pre-condition showed a minimal creep strength that ranged between 0.053 and 0.077. This represents very minimal creep over the course of the test. For the 11.0 pH pre-condition the creep strength was very consistent for all stress levels tested at 0.130. This represented noticeable creep over the time period tested.

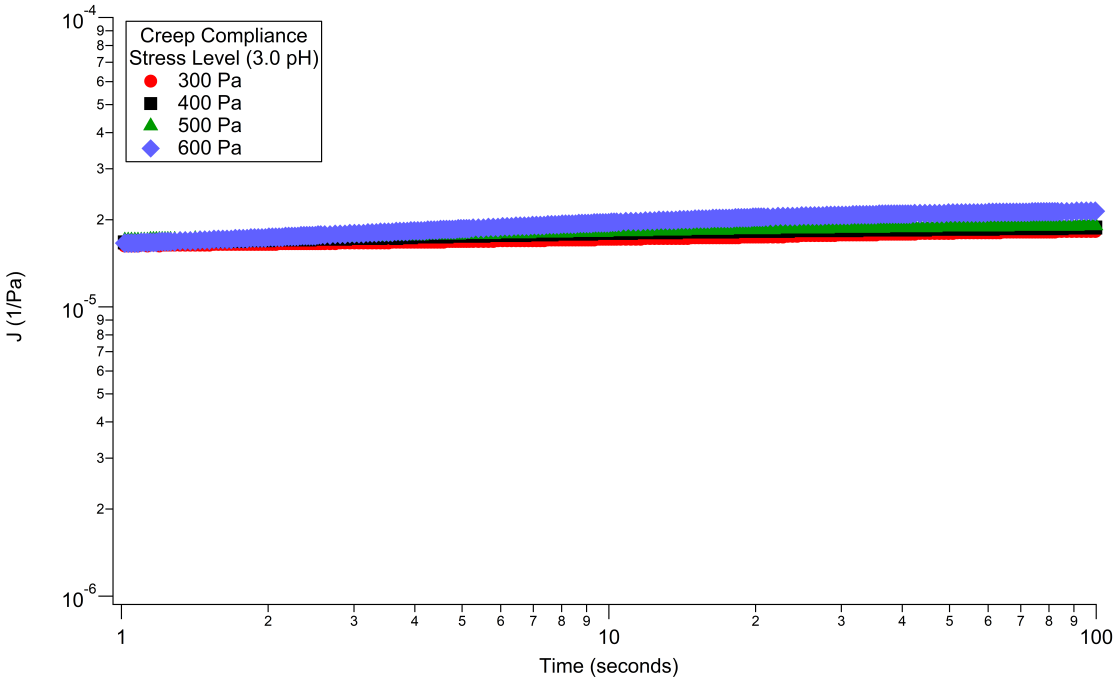

FIGURE 2.4: Creep compliance for 3.0 pH pre-swollen samples.

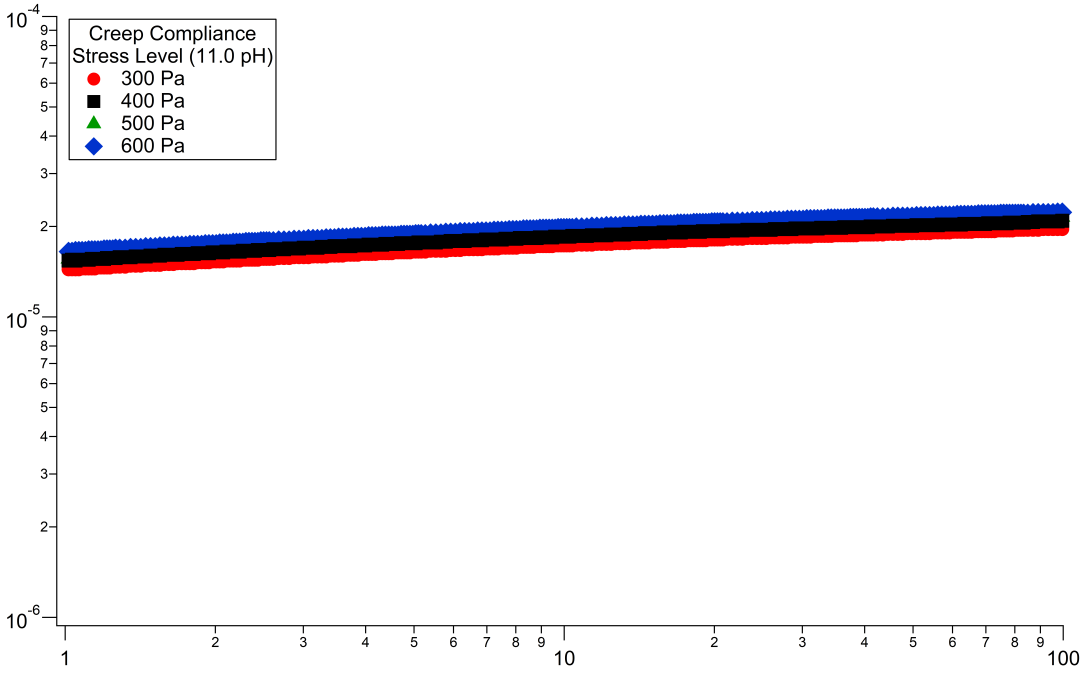

FIGURE 2.5: Creep compliance for 11.0 pH pre-swollen samples.

3.0 pH		
Stress Level (Pa)	A $(10^{-5})(1/Pa/s)$	n
300	1.55±0.71	0.053±0.011
400	1.59±0.46	0.055±0.017
500	1.61±0.79	0.056±0.008
600	1.61±0.46	0.077±0.025

TABLE 2.1: Creep compliance fit to a power law funtion $J(t) = At^n$ for the 3.0 pH pre-condition. The variable n represents the creep strength.

11.0 pH		
Stress Level (Pa)	A $(10^{-5})(1/Pa/s)$	n
300	1.30±0.19	0.130±0.014
400	1.37±0.41	0.129±0.006
500	1.40±0.23	0.131±0.011
600	1.47±0.49	0.130±0.011

TABLE 2.2: Creep compliance fit to a power law funtion $J(t) = At^n$ for the 11.0 pH pre-condition. The variable n represents the creep strength.

2.6 Discussion

The present gels may be compared with selected polymers. Hevea rubber, [8] has a Young's modulus of about 1 MPa and tan δ on the order of 0.01 to 0.05 at low frequencies at room temperature. Neoprene rubber has a loss tangent of 0.1 to 0.15 at room

temperature, up to about 100 Hz. Rubbery materials (elastomers) intended for for vibration damping and impact absorption [27] can have larger tan δ exceeding 1 over a narrow range of temperature and frequency.

Comparison with soft tissue may be pertinent to some applications of the gels. Human abdominal fat tissue exhibits a shear storage modulus [24] of 1.8 to 3.4 kPa at angular frequencies 0.1 to 50 rad/s, with tan δ of about 0.25. These authors also studied hydrogels; a of poly(ethylene glycol) diacrylate hydrogel exhibited a shear modulus of about 10 kPa and tan δ of about 0.1.

Dynamic rheology tests were completed on HEMA-DMAEMA responsive hydrogels pre-swollen in 3.0 pH and 11.0 pH buffer solution respectively. The hydrogel has a low loss modulus when pre-swollen in 3.0 pH buffer solution and the measured value for tan(δ) did not vary substantially with changes in frequency. When the gel was pre-swollen in 11.0 pH buffer solution there is a significant upward shift in the loss modulus and the material displayed more viscoelastic characteristics. The damping of the gel showed a frequency dependence with a monotonic increase in tan(δ) with increasing frequency. The observed behavior indicates a pH dependence in the dynamic moduli of the material. This increased viscoelastic behavior was definitely observed as the frequency of displacements was increased.

When pre-conditioned in 3.0 pH buffer solution the hydrogel has undergone several chemical reactions that increase the water content in the hydrogel. In addition to normal diffusion of H_2O water is being formed by chemical reactions inside the hydrogel. These

chemical reactions expand the cross-linked network. This network finds an equilibrium conformational configuration. In this expanded state the network cross-links are not able to slide and flow with respect to one another. This would give the hydrogel its 'elastic' solid like behavior when swollen in 3.0 pH. When the hydrogel is pre-conditioned in 11.0 pH buffer solution no chemical reactions are occurring with the diffusion of ionic species into the hydrogel. The network cross-links are allowed to move to a much greater extent with respect to one another and still maintain the hydrogels cross-link density. This gives the hydrogel its viscoelastic properties in this regime while maintaining its solid form based on the cross-linked nature of the hydrogel.

Studies of dex-HEMA-MAA/HEMA-DMAEMA with a solid content of (15%) showed a tan(δ) of about 0.060 at 1% strain taken at room temperature[28]. This compares well to the tan(δ) measured at 0.069 for 1% strain taken at 1 Hz in frequency when swollen in 3.0 pH buffer solution. In contrast the hydrogel has a loss tangent of 0.42 for 1% at 1 Hz for the samples swollen in 11.0 pH buffer solution. Poly(methyl methacrylate) - poly(dimethyl amino ethyl methacrylate) - poly (methyl methacrylate) PMMA-PDMAEMA-PMMA, which is itself a responsive polymer, has a measured value for G' of $\approx$ 120 Pa and loss modulus of $\approx$ 10 Pa tested at 3.5 pH, (adapted from [4]) which is significantly softer than the HEMA-DMAEMA tested at 3.0 pH which has a G' of 41$\pm$9.1 kPa and a G'' of 2.7$\pm$0.62 kPa for 1% at 1 Hz.

2.7 Conclusion

This study explained the viscoelastic behavior of HEMA-DMAEMA stimuli-responsive hydrogels swollen in 3.0 pH and 11.0 pH buffer solutions. These stimuli-responsive hydrogels displayed different behavior when external environments changed from acidic to basic solutions. This study expands our knowledge and understanding of HEMA-DMAEMA viscoelastic behavior in two different external environmental conditions. Additionally the study provides data for more efficient device design in microfluidic devices.

2.8 Acknowledgments

I would like to acknowledge helpful conversations that I have had with fellow graduate student Mehrdad Arjmand, and professor Walter Drugan. Additionally I would like to acknowledge professor Lih-Sheng Turng and Bionates for the use of his rheometer during dynamic testing and undergraduate student Rachel Craven for the work she performed assisting in rheometry testing.

Bibliography

[1] Abhishek K Agarwal, Sudheer S Sridharamurthy, David J Beebe, and Hongrui Jiang. Programmable autonomous micromixers and micropumps. *Journal of microelectromechanical systems*, 14(6):1409–1421, 2005.

[2] Joseph D Andrade. *Hydrogels for medical and related applications*. ACS Publications, 1976.

[3] David J Beebe, Jeffrey S Moore, Joseph M Bauer, Qing Yu, Robin H Liu, Chelladurai Devadoss, and Byung-Ho Jo. Functional hydrogel structures for autonomous flow control inside microfluidic channels. *Nature*, 404(6778):588–590, 2000.

[4] Frédéric Bossard, Thierry Aubry, Georgios Gotzamanis, and Constantinos Tsitsilianis. ph-tunable rheological properties of a telechelic cationic polyelectrolyte reversible hydrogel. *Soft Matter*, 2(6):510–516, 2006.

[5] Liang Dong and Hongrui Jiang. Autonomous microfluidics with stimuli-responsive hydrogels. *Soft matter*, 3(10):1223–1230, 2007.

[6] Liang Dong, Abhishek K Agarwal, David J Beebe, and Hongrui Jiang. Adaptive liquid microlenses activated by stimuli-responsive hydrogels. *Nature*, 442(7102):551–554, 2006.

[7] Liang Dong, Abhishek K Agarwal, David J Beebe, and Hongrui Jiang. Variable-focus liquid microlenses and microlens arrays actuated by thermoresponsive hydrogels. *Advanced Materials*, 19(3):401–405, 2007.

[8] J.D. Ferry. Viscoelastic Properties of Polymers, 2nd ed. J. Wiley, NY, 1970.

[9] PJ Flory. Principles of polymer chemistry (cornell university, ithaca, 1953). *Statistical Mechanics of Chain Molecules*, 1969.

[10] Gerald Gerlach, Margarita Guenther, Joerg Sorber, Gunnar Suchaneck, Karl-Friedrich Arndt, and Andreas Richter. Chemical and ph sensors based on the swelling behavior of hydrogels. *Sensors and Actuators B: Chemical*, 111:555–561, 2005.

[11] Piyush Gupta, Kavita Vermani, and Sanjay Garg. Hydrogels: from controlled release to ph-responsive drug delivery. *Drug discovery today*, 7(10):569–579, 2002.

[12] Alex J Hughes, Robert KC Lin, Donna M Peehl, and Amy E Herr. Microfluidic integration for automated targeted proteomic assays. *Proceedings of the National Academy of Sciences*, 109(16):5972–5977, 2012.

[13] Kenneth T Kotz, Wenzong Xiao, Carol Miller-Graziano, Wei-Jun Qian, Aman Russom, Elizabeth A Warner, Lyle L Moldawer, Asit De, Paul E Bankey, Brianne O Petritis, et al. Clinical microfluidics for neutrophil genomics and proteomics. *Nature medicine*, 16(9):1042–1047, 2010.

[14] James R Kraly, Ryan E Holcomb, Qian Guan, and Charles S Henry. Microfluidic applications in metabolomics and metabolic profiling. *Analytica chimica acta*, 653 (1):23–35, 2009.

[15] RS Lakes. *Viscoelastic materials*. Cambridge University Press, 2009.

[16] Dong Liang, Abhishek K Agarwal, David J Beebe, and Hongrui Jiang. Adaptive liquid microlenses activated by stimuli-responsive hydrogels. *Nature*, 442(7102):551, 2006.

[17] Niels Lion, Tatiana C Rohner, Loic Dayon, Isabelle L Arnaud, Eugen Damoc, Nikolay Youhnovski, Zhi-Yong Wu, Christophe Roussel, Jacques Josserand, Henrik Jensen, et al. Microfluidic systems in proteomics. *Electrophoresis*, 24(21):3533–3562, 2003.

[18] Chi-Wei Lo, Difeng Zhu, and Hongrui Jiang. An infrared-light responsive graphene-oxide incorporated poly (n-isopropylacrylamide) hydrogel nanocomposite. *Soft Matter*, 7(12):5604–5609, 2011.

[19] Shingo Maeda, Yusuke Hara, Ryo Yoshida, and Shuji Hashimoto. Active polymer gel actuators. *International journal of molecular sciences*, 11(1):52–66, 2010.

[20] Renate Messing and Annette M Schmidt. Perspectives for the mechanical manipulation of hybrid hydrogels. *Polymer Chemistry*, 2(1):18–32, 2011.

[21] Peter Mitchell. Microfluidics–downsizing large-scale biology. *Nature biotechnology*, 19(8):717, 2001.

[22] Mikhail Motornov, Yuri Roiter, Ihor Tokarev, and Sergiy Minko. Stimuli-responsive nanoparticles, nanogels and capsules for integrated multifunctional intelligent systems. *Progress in polymer science*, 35(1):174–211, 2010.

[23] George Pasparakis and Maria Vamvakaki. Multiresponsive polymers: nano-sized assemblies, stimuli-sensitive gels and smart surfaces. *Polymer Chemistry*, 2(6):1234–1248, 2011.

[24] P. N. Patel, C. K. Smith, and C. W. Jr. Patrick. Rheological and recovery properties of poly(ethylene glycol) diacrylate hydrogels and human adipose tissue.

[25] Nicholas A Peppas. *Hydrogels in medicine and pharmacy: properties and applications*, volume 3. CRC PressI Llc, 1987.

[26] Robert Plunkett. Damping analysis: an historical perspective. In *M 3 D: Mechanics and Mechanisms of Material Damping*. ASTM International, 1992.

[27] J.C. Snowdon. *Vibration and Shock in Dampled Mechanical Systems*. J. Wiley, NY, 1968.

[28] Sophie R Van Tomme, Mies J van Steenbergen, Stefaan C De Smedt, Cornelus F van Nostrum, and Wim E Hennink. Self-gelling hydrogels based on oppositely charged dextran microspheres. *Biomaterials*, 26(14):2129–2135, 2005.

[29] George M Whitesides. The origins and the future of microfluidics. *Nature*, 442(7101): 368–373, 2006.

[30] Kazumasa Yamaki, Ichiro Harada, Mitsuaki Goto, Chong-Su Cho, and Toshihiro Akaike. Regulation of cellular morphology using temperature-responsive hydrogel for integrin-mediated mechanical force stimulation. *Biomaterials*, 30(7):1421–1427, 2009.

[31] Chae YunáBae et al. User-friendly 3d bioassays with cell-containing hydrogel modules: narrowing the gap between microfluidic bioassays and clinical end-users' needs. *Lab on a Chip*, 15(11):2379–2387, 2015.

Chapter 3

Implicit Elasticity of HEMA-DMAEMA

3.1 Introduction

In this paper we show a method of measuring the Fung parameter for pH sensitive 2-hydroxyethyl methacrylate (2 - dimethylamino) ethyl methacrylate (HEMA-DMAEMA) stimuli-responsive hydrogel through a simple tension test. The Fung parameter defined in Eq. 3.3 is a measure of the relative nonlinear coupling between stress and strain and is used primarily in implicit elastic formulations. The Fung parameter is then compared to tension testing data for HEMA-DMAEMA hydrogels pre-conditioned in 3.0 pH (swollen) and 11.0 pH (unswollen) buffer solutions.

In the microfluidics domain stimuli-responsive hydrogels are used as sensors and actuators because of the ease of fabrication and the natural actuation of the material when an external stimulus is supplied[2, 22]. HEMA-DMAEMA stimuli-responsive hydrogels are cross-linked copolymers formed by free radical polymerization[17]. Polymers that are stimuli-responsive can swell or shrink when introduced to external stimuli such as changes in temperature, pH, or electric field[29].

These polymers find uses in a wide range of scientific fields such as medical devices[21], controlled drug delivery[5, 10, 25], and self-responsive actuators and sensors[2, 7, 8], microfluidic flow[2], bio-inspired muscle like actuators[4, 26], and bending mode actuators[18] in addition to many others. Characterization of the mechanical properties of these materials with respect to changing environmental conditions is important to the applications listed above.

The distribution of ionic charges in pH sensitive hydrogels have a role in their swelling behavior. There have been two main schools of thought concerning how this ionic distribution of charges effects deformation of the hydrogel. One is a stress distribution due to osmotic pressure[11, 12] and another accounts for the effects of electrostatic repulsion[24]. Many researchers have gone back and forth on these two field theories debating the validity of both. More recently field theories have been developed to try and couple the ionic and mass transport with deformation in the hydrogel[1, 6, 9, 20, 31].

In 2002 De et al.[6] modeled the stresses in the hydrogel as a system of partial differential equations that coupled diffusion with electrostatics which then coupled electrostatics with

osmotic pressure. The osmotic pressure was then coupled to the stress field through the displacement field. This was one of the first papers to incorporate this methodology for the study of pH sensitive responsive hydrogels.

In 2004 Baek and Srinivasa modeled the swelling of ionic gels immersed in a diffusing solvent of varying pH by applying a variational method[1]. In this model the coupling of all the different physical phenomenon was done through an appropriately selected strain energy density function that was thermodynamic in origin. The strain energy function was written as a sum of the strain energy due to swelling and ionic migration. The strain energy due to ionic migration is a function of the ions in the solvent and the bound charges on the polymer chains of the hydrogel.

In 2008 Hong et al. proposed a strain energy density function that consisted of four terms. These were the strain energies due to swelling, mixing, ionic migration and charge disassociation[20]. As theories have become more sophisticated they have also become more complicated. Term after term is added to strain energy functions in an attempt to get them to match experimental data. These formulations all have one thing in common, they are explicit elastic formulations. The stress can be completely described by the gradient of a potential energy function that is itself solely a function of strain.

This assumption indicates that the stress fields generated within the hydrogel as a result of applied forces has a singular general form that is not influenced by boundary conditions and/or prior states of stress. For short times, or minimal growth this assumption is valid. However, in the case of pH sensitive hydrogels that swell to more than 10% of their

original volume, such as HEMA-DMAEMA hydrogel formulations, this assumption does not hold.

What is not debated in any of the theories cited above is the fact that diffusion of ionic species affects stresses generated within hydrogels. The diffusion is geometrically dependent. An argument can be made that the stresses in these hydrogels are not explicitly determined by an accompanying strain field. These stresses are governed not only by strains but by the history of stress the material has undergone. It can be stated that the current stress is an implicit function of prior stress and strain.

In 2003 Rajagopal[27] described a class of materials that are not explicit functions of strain, as is the case with hyperelastic field theories, but are implicit functions of stress and strain. He coined the term 'Implicit' elasticity. Much earlier, in 1967, Y.C. Fung proposed an empirical law that governed the one dimensional passive response of non-linear soft tissues[16],

$$\frac{dS(\lambda)}{d\lambda} = a(S(\lambda) + \beta), \tag{3.1}$$

where $S(\lambda)$ is the 2nd Piola-Kirchoff stress, λ is the stretch which is final length over initial length and a and β are material parameters. This equation is referred to as Fung's Law. Upon closer inspection if written in its rate form,

$$dS(\lambda) = a\beta d\lambda + aS(\lambda)d\lambda, \tag{3.2}$$

one can see that this equation has a linear and non-linear elastic term. The parameter $a\beta$ is analogous to a Young's modulus like term and has the dimensions of stress while the parameter a is a dimensionless term that measures the degree of coupling between stress and strain. Re-writing Fung's law and renaming the material parameters,

$$\frac{dS(\lambda)}{d\lambda} = E^{\circ} + \beta^{\circ} S(\lambda), \tag{3.3}$$

where E° represents an elastic modulus and β° is a term known as the Fung parameter. Fung's law is one of the first proposed implicit elastic formulations and is used in the field of biomechanics to describe the one dimensional stress response of soft materials as a function of stretch. As an implicit elastic extension of Fung's law into three dimensions, Freed[13] proposed an implicit elastic constitutive equation to describe the behavior of soft solid materials and it is this constitutive equation that is used in this work to determine the Fung parameter β°.

3.1.1 Implicit Elasticity

For soft materials the main contribution to the potential energy $\mathscr{E}$ contained in a particle is due to an entropic process. For stimuli-responsive hydrogels this entropic process can have many contributions. HEMA-DMAEMA hydrogels are responsive to a change in the pH of the external environment. This causes the hydrogel to increase in volume and the stress field generated is due to the diffusion of solution into the gel and the subsequent

stretching of the cross-linked network. The diffusion is geometry dependent and thus the osmotic pressure and overall stress field generated is geometry dependent. The strain energy density, in this situation, is a function not only of strain but of the prior state of stress. Therefore the strain energy density takes the form $\mathscr{E} = W(\mathbf{E}, \mathbf{S}; \mathbf{C})$ and the *Clausius-Planck* inequality[13, 19] takes the form,

$$\mathscr{D} = tr(\mathbf{S}d\mathbf{E}) - dW(\mathbf{E}, \mathbf{S}; \mathbf{C}), \tag{3.4}$$

in which $\mathbf{S}$ is the second Piola-Kirchoff stress tensor and $\mathbf{E}$ is the Green-Cauchy strain tensor defined as, $\mathbf{E} = (1/2)(\mathbf{C} - \mathbf{I})$, where $\mathbf{I}$ is the identity tensor and $\mathbf{C}$ is the Green deformation tensor defined as $\mathbf{C} = \mathbf{F^T F}$. All quantities defined with a bold face type are tensor quantities, and in equation (3.4) the ; in $dW(\mathbf{E}, \mathbf{S}; \mathbf{C})$ is a reference to whether the formulation is Lagrangian or Eulerian. In finite elasticity reference frame does make a difference and for implicit elasticity formulations the history of stress is taken from an initial reference to a current reference frame so the formulation should inherently be Lagrangian. For a completely elastic response the dissipation $\mathscr{D}$ is zero. The strain energy density can then be expanded via the chain rule to give,

$$dW = \frac{\partial W}{\partial \mathbf{E}} d\mathbf{E} + \frac{\partial W}{\partial \mathbf{S}} d\mathbf{S}. \tag{3.5}$$

With the following relationship $tr(\mathbf{S}d\mathbf{E}) = \mathbf{S} \cdot\cdot d\mathbf{E}$, equation (3.5) is used in equation (3.4) with the dissipation set to zero yields the following result,

$$\frac{\partial^2 W}{\partial \mathbf{S}\partial \mathbf{S}} \cdot\cdot d\mathbf{S} = \left(\mathbf{I} - \frac{\partial^2 W}{\partial \mathbf{S}\partial \mathbf{E}}\right) \cdot\cdot d\mathbf{E}. \tag{3.6}$$

Solving for the stress rate $d\mathbf{S}$ we have the following relationship,

$$d\mathbf{S} = \left(\frac{\partial^2 W}{\partial \mathbf{S}\partial \mathbf{S}}\right)^{-1} : \left(\mathbf{I} - \frac{\partial^2 W}{\partial \mathbf{S}\partial \mathbf{E}}\right) \cdot\cdot d\mathbf{E}. \tag{3.7}$$

The quantity $\left(\frac{\partial^2 W}{\partial \mathbf{S}\partial \mathbf{S}}\right)^{-1} : \left(\mathbf{I} - \frac{\partial^2 W}{\partial \mathbf{S}\partial \mathbf{E}}\right)$ is known as the *tangent modulus* and equation (3.7) is often written as,

$$d\mathbf{S} = \mathscr{M} \cdot\cdot d\mathbf{E}. \tag{3.8}$$

Equation (3.8) defines an *implicit elastic solid*[13, 27]. For HEMA-DMAEMA stimuli responsive hydrogels the stress field is diffusion dependent and thus the stress field and deformation is time dependent. It can be assumed that the potential energy function (strain energy density function) is independent of time and the tangent modulus defined in equation (3.7) is subsequently independent of time. Thus we define the constitutive rate equation for the HEMA-DMAEMA hydrogel to be,

$$d\dot{\mathbf{S}} = \mathscr{M} \cdot\cdot d\dot{\mathbf{E}}. \tag{3.9}$$

This is a general constitutive rate equation for an implicit elastic solid.

3.1.2 Sample Preparation

A prepolymer solution is prepared using the reagents, 2-(dimethylamino) ethyl methacrylate (DMAEMA), 2-hydroxyethl methacrylate (HEMA), ethylene glycol dimethacrylate (EGDMA) and 2,2-dimethoxy-2-phenylacetophenone (DMPA). The reagents are mixed together in the following ratios, 25.77:5.718:0.467:1. All reagents were purchased from Sigma-Aldrich. Prior to polymerization this hydrogel-liquid solution is stored at $-8°C$.

For tensile testing samples A type IV sample size was used based on ASTM D 638-99 standards[30]. Samples were fabricated with a total length of 40 mm, a gauge length of 8.0 mm, a gauge width of 1.5 mm and a thickness of 1.0 mm.

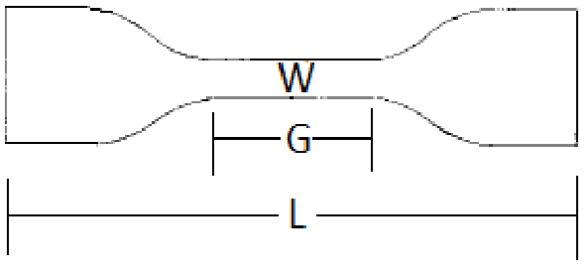

FIGURE 3.1: A type IV ASTM D 638-99 tensile testing sample schematic[30]. W is the gauge width of 1.5 mm, G is the gauge length of 8.0 mm and L is the total sample length of 40 mm. The thickness of each sample is 1.00 mm[30]

A PDMS stencil was produced by a compression molding process that makes use of a negative-tone UV photoresist silicon wafer with the requisite pattern. The PDMS stencil was placed on top of a flat PDMS substrate. The stencil channels were filled with the HEMA-DMAEMA pre-polymer solution. A third layer of PDMS was placed on top of the stencil. The pre-polymer solution is then exposed to UV light at an intensity

of 20 mW/cm^2 for a total of 120 seconds[23]. Cross-head displacements are used to determine the stretch and these stretch measurements are used to calculate Green strain, $E_z = (1/2)(\lambda^2 - 1)$ where E_z is Green strain along the z-axis and λ is stretch measured as final length over initial length.

A 5548 Instron micro-tester is used to record load measurements during tension experiments. The Instron micro-tester is equipped with a 10 N load cell. The load cell has automatic transducer recognition and an accuracy of 1/500th of the load capacity.

3.1.3 Determination of Fung Parameter

Experiments were performed on HEMA-DMAEMA stimuli-responsive hydrogels to determine the Fung parameter β°. Responsive hydrogels are inherently non-linear materials, however the stress/strain plot of the hydrogel in one dimensional tensile testing shows that under low strains, < 5 %, the material behaves like a Hookean solid. In this region of interest the Young's modulus and Poisson ratio have meaning. Tensile tests are used to determine these mechanical properties. Above 5% strain the non-linear behavior of the hydrogel is exhibited. Tensile tests in this range, as shown in figure 3.2, are used to determine the Fung parameter β° that will be used in model validation.

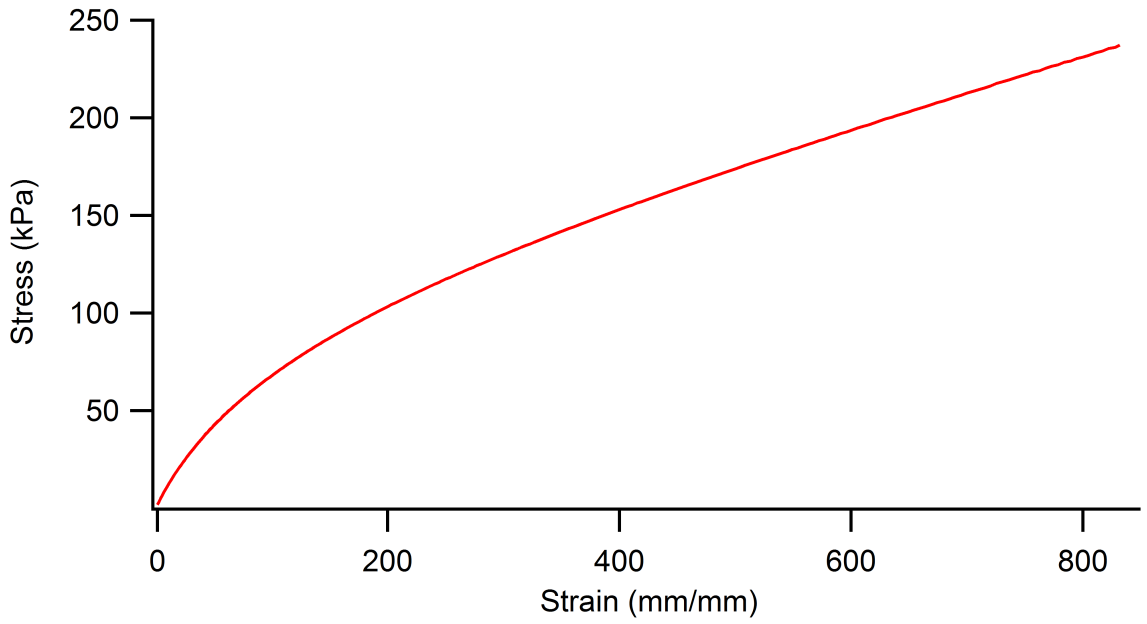

FIGURE 3.2: A representative stress vs. strain curve for HEMA-DMAEMA testing in tension at a rate of 5 mm/min.

For explicit elastic materials, also known as hyperelastic materials, there exists a potential energy function that is only a function of strain. This is known as the strain energy function $W(\mathbf{E})$ and the constitutive relationship is given as[33],

$$\mathbf{S} = \frac{\partial W(\mathbf{E})}{\partial \mathbf{E}}, \tag{3.10}$$

For Hookean solids under the assumption of small strains we can write the constitutive relationship as,

$$\sigma_{ij} = C_{ijkl}\varepsilon_{kl}, \tag{3.11}$$

where C_{ijkl} is the fourth order modulus tensor that contracts the stress with strain. For linear elastic materials this modulus tensor is constant valued and is positive definite. The positive definite characteristic of the modulus tensor gives rise to bounds for material properties defined within. Thus the Poisson ratio is bounded between -1 and 1/2 and the Young's modulus is always positive. When strains become large the stress strain relationship becomes non-linear and the concept of a Young's modulus loses meaning as a parameter that can characterize the entire evolution of stress and strain. The modulus that contracts stress with strain can become a function of the prior state of strain. The modulus tensor can be thought of as a linearized version of the tangent modulus. For implicit elastic solids the modulus that contracts stress with strain can be a function of the prior state of stress in addition to the prior state of strain. Let us consider the constitutive equation (3.8), which in component form is,

$$dS_{ij} = M_{ijkl} dE_{kl}, \tag{3.12}$$

where the tangent modulus M_{ijkl} is given by,

$$\mathbf{M} = \left(\frac{\partial^2 W}{\partial \mathbf{S} \partial \mathbf{S}} \right)^{-1} : \left(\mathbf{I} - \frac{\partial^2 W}{\partial \mathbf{S} \partial \mathbf{E}} \right). \tag{3.13}$$

The tangent modulus M_{ijkl} is non-linear function of stretch and depends on the prior state of stress. For convenience we rename the two second order derivatives of the strain energy function as,

$$\mathscr{A} = \frac{\partial^2 W}{\partial \mathbf{S} \partial \mathbf{S}}, \tag{3.14}$$

and

$$\mathscr{B} = \frac{\partial^2 W}{\partial \mathbf{S} \partial \mathbf{E}}, \tag{3.15}$$

and the tangent modulus can be rewritten as,

$$\mathbf{M} = \mathscr{A}^{-1} : (\mathbf{I} - \mathscr{B}). \tag{3.16}$$

The responsive hydrogel HEMA-DMAEMA exhibits stress/strain behavior that is linear at small strains and becomes non-linear at large strains. The hydrogel can undergo large reversible volumetric deformations caused by the diffusion and creation of H_2O within the polymeric environment and increases in osmotic pressure of the diffusing ionic species. The growth of the hydrogel is coupled with governing diffusion equations to account for these two phenomena. We now postulate the existence of a strain energy function of the implicit form as given by Freed[13],

$$W(\mathbf{E}, \mathbf{S}; \mathbf{C}) = \frac{-\nu}{2E}(S_{mn}C_{nm})^2 + \frac{1+\nu}{2E}S_{mn}C_{np}S_{pq}C_{qm} - \frac{\beta^\circ}{2E}S_{mn}E_{np}S_{pq}C_{qm}, \tag{3.17}$$

where ν and E are the familiar Poisson ratio and Young's modulus from mechanics of materials and β° is the Fung parameter. This form of the strain energy function takes into account the linear behavior of the gel at low strains and the non-linear behavior of the gel at large strains. The fourth order tensors $\mathscr{A}$ and $\mathscr{B}$ take the form,

$$\mathscr{A} = \frac{-\nu}{E} C_{ji} C_{lk} + \frac{1+\nu}{E} C_{li} C_{jk} - \frac{\beta^\circ}{2E} (E_{li} C_{jk} + C_{li} E_{jk}), \tag{3.18}$$

and,

$$\mathscr{B} = \frac{-\beta^\circ}{2E} (\delta_{jk} S_{lp} C_{pi} + \delta_{il} S_{mk} C_{jm}) \tag{3.19}$$

To determine the Young's and shear modulus used for material characterization we use a well known formulation from rubber elasticity[32]. For axial deformation the constitutive equation is given as,

$$\sigma = G(\lambda - \lambda^{-2}), \tag{3.20}$$

where G is the shear modulus and λ is the stretch. This formulation is only valid for a cross-linked elastomer. This equation has proven to be successful in fitting experimental data at small strains. An apparent Young's modulus is formulated from the measured shear modulus G via,

$$E_a = 3G, \tag{3.21}$$

The apparent modulus E_a is thus named because the concept of a Young's modulus fails to capture the mechanics taking place in soft materials. The standard engineering Young's modulus is a parameter that is only valid at low strains. At finite strains the value of the Young's modulus can change for different loading conditions and it cannot capture accurately the stress/strain relationships taking place. For uniaxial tension over the course of moderate strains ($\leq$80%) the shear modulus calculated from equation (3.20), yields the apparent modulus E_a for incompressible materials.

3.1.4 Fung Parameter

Using the compliance tensor $\mathbf{J_c} = \mathbf{M}^{-1}$ given as,

$$\mathbf{J_c} = \begin{pmatrix} \frac{\beta^\circ {\lambda_1}^2 - (\beta^\circ - 2){\lambda_1}^4}{2\left(S_{11}\beta^\circ {\lambda_1}^2 + E\right)} & -\frac{{\lambda_1}^2 {\lambda_2}^2 \nu}{S_{11}\beta^\circ {\lambda_1}^2 + E} & -\frac{{\lambda_1}^2 {\lambda_3}^2 \nu}{S_{11}\beta^\circ {\lambda_1}^2 + E} \\ -\frac{{\lambda_1}^2 {\lambda_2}^2 \nu}{S_{22}\beta^\circ {\lambda_2}^2 + E} & \frac{\beta^\circ {\lambda_2}^2 - (\beta^\circ - 2){\lambda_2}^4}{2\left(S_{22}\beta^\circ {\lambda_2}^2 + E\right)} & -\frac{{\lambda_2}^2 {\lambda_3}^2 \nu}{S_{22}\beta^\circ {\lambda_2}^2 + E} \\ -\frac{{\lambda_1}^2 {\lambda_3}^2 \nu}{S_{33}\beta^\circ {\lambda_3}^2 + E} & -\frac{{\lambda_2}^2 {\lambda_3}^2 \nu}{S_{33}\beta^\circ {\lambda_3}^2 + E} & \frac{\beta^\circ {\lambda_3}^2 - (\beta^\circ - 2){\lambda_3}^4}{2\left(S_{33}\beta^\circ {\lambda_3}^2 + E\right)}, \end{pmatrix} \tag{3.22}$$

where λ_i given $i = 1, 2, 3$, are the principle stretches, E is the Young's modulus, S_{ii} are the principle 2nd Piola-Kirchoff stresses and β° is the Fung parameter. Determination of the Fung parameter β° is done using the relationship,

$$\mathbf{dE} = \mathbf{J_c dS} \tag{3.23}$$

For a tensile test the material is strained axially and load is recorded, because there is no stress in the lateral and transverse directions we can take the J_{c11} term and get the following,

$$\mathbf{dE_{11}} = \frac{\beta^\circ(\lambda^2 - \lambda^4) + 2\lambda^4}{2(S_{11}\beta^\circ\lambda^2 + E)}\mathbf{dS_{11}}, \tag{3.24}$$

where $d\mathbf{E_{11}}$ is the change in strain in the axial direction, $d\mathbf{S_{11}}$ is the change in the 2nd Piola-Kirchoff stress in the axial direction, λ is the stretch in the axial direction, S_{11} is the prior stress in the axial direction and E is the Young's modulus. The Fung parameter β° can be solved for using equation (3.25),

$$\beta^\circ[2S_{11}\lambda^2\mathbf{dE_{11}} + (\lambda^4 - \lambda^2)\mathbf{dS_{11}}] = 2[\lambda^4\mathbf{dS_{11}} - E\mathbf{dE_{11}}], \tag{3.25}$$

Experimentally we need to determine the Fung parameter β. The process can be simplified by re-writing equation (3.25) as follows,

$$B_o = \beta^\circ A_o, \tag{3.26a}$$

$$A_o = 2S_{11}\lambda^2 \mathbf{dE_{11}} + (\lambda^4 - \lambda^2)\mathbf{dS_{11}}, \tag{3.26b}$$

$$B_o = 2[\lambda^4 \mathbf{dS_{11}} - E\mathbf{dE_{11}}]. \tag{3.26c}$$

Equation (3.26b) is plotted against equation (3.26c) and the slope of the linear region is the Fung parameter β°.

3.2 Results

Tensile testing in both the swollen and unswollen states was performed to also determine the Young's modulus E, the shear modulus G, and Poisson's ratio ν used to determine the Fung parameter β°.

In figure 3.3 the shear modulus is determined using equation (3.20). It should be noted that equation (3.20) only yields the shear modulus for small strains under uni-axial tension. This is a feature unique to elastomers. The assumption of incompressibility is made and the apparent Young's modulus is given as, $E_a = 3G$.

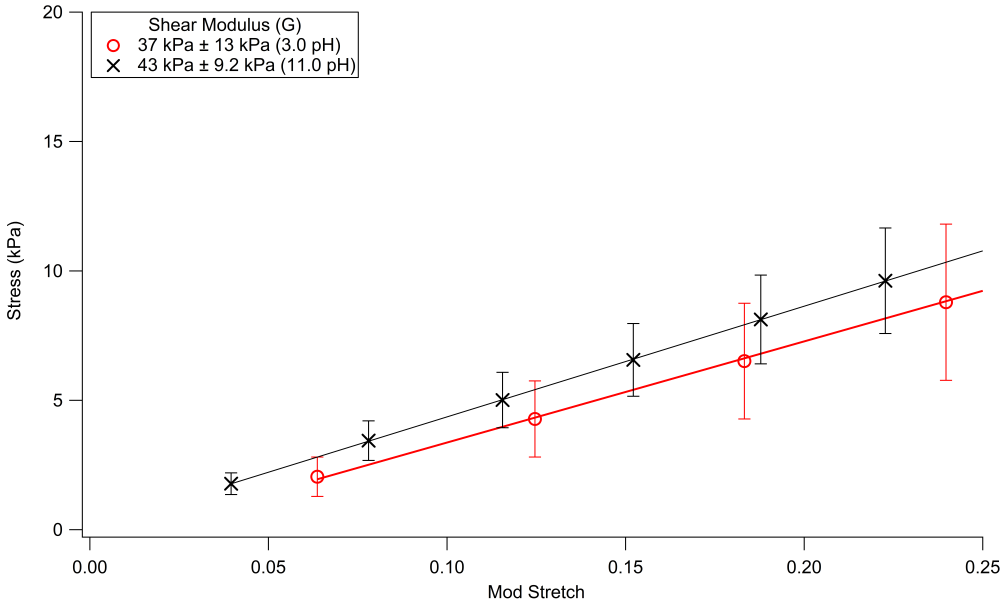

FIGURE 3.3: Measurement of the Shear modulus. Mod Stretch is defined as $(\lambda - \lambda^{-2})$ from equation (3.20). The samples pre-conditioned in 3.0 pH and 11.0 pH buffer solution and the modulus is calculated over the first 10% of strain.

The Young's modulus calculated for samples pre-swollen in 11.0 pH buffer solution is 129 kPa and the shear modulus is 43±9.2 kPa. For the samples pre-swollen in 3.0 pH buffer solution the Young's modulus is 111 kPa and the shear modulus is 37±13 kPa.

The Fung parameter is determined by plotting equation (3.26b) against equation (3.26c). The slope of this plot is the Fung parameter for HEMA-DMAEMA stimuli-responsive hydrogels under uni-axial tension. The parameter is determined using the J_{c11} term from the compliance tensor for the three dimensional implicit elastic consitutive equation proposed by Freed[13].

In figure 3.4 the Fung parameter is determined from the average value of the slopes of the B_o and A_o plots. The Fung parameter β° is measured to be 0.870 ± 0.018.

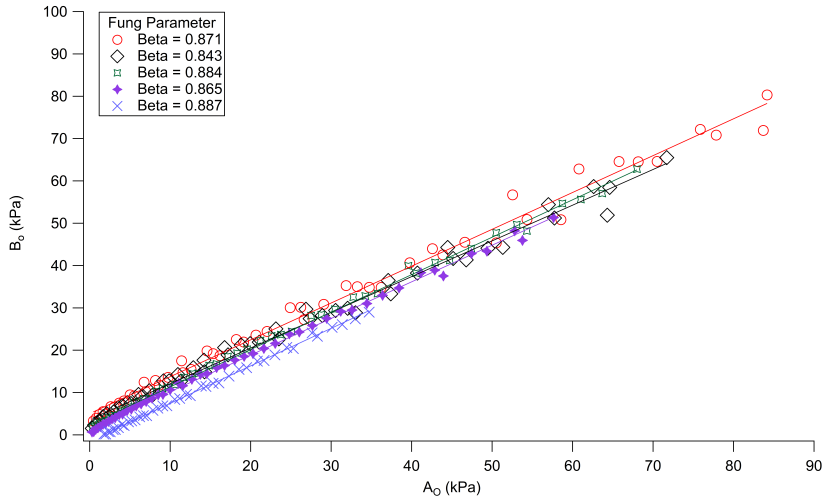

FIGURE 3.4: Test for β parameter. These samples were pre-conditioned in 7.0 pH buffer solutions prior to testing. The 7.0 pH buffer solution is neutral and does not initiate swelling in the material.

Figures 3.5 and 3.6 show the theoretical predictions compared to the experimental data for the 3.0 pH and 11.0 pH pre-conditions respectively.

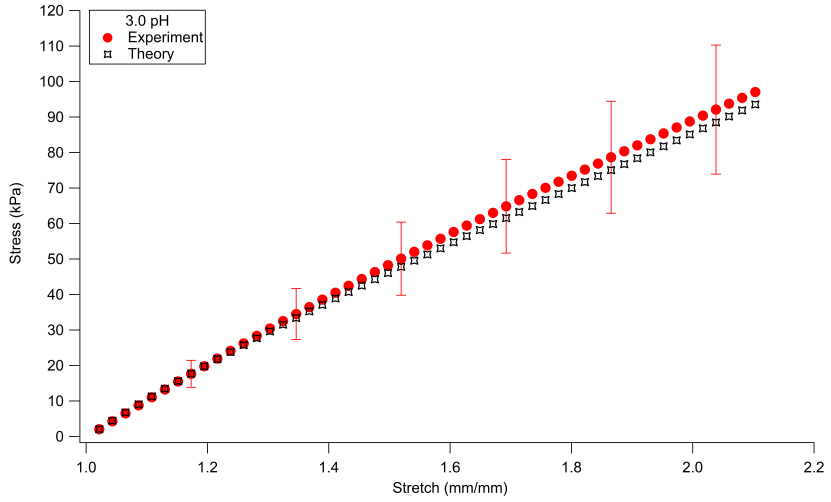

FIGURE 3.5: Average stress vs stretch data for 3.0 pH pre-conditioning. The average is taken from N = 5, for each test condition.

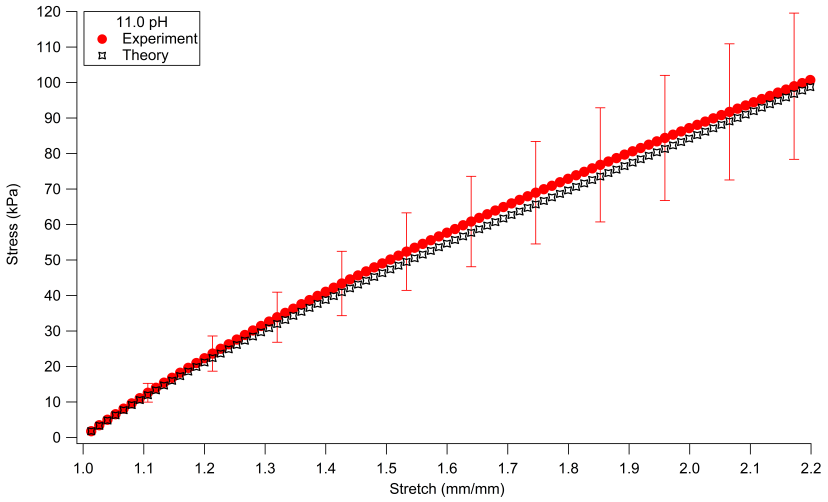

FIGURE 3.6: Average stress vs stretch data for 11.0 pH pre-conditioning. The average is taken from N = 4, for each test condition.

3.3 Discussion

Theories that describe hydrogel swelling have many things in common. They are in general a complicated set of partial differential field equations that couple diffusion, electrostatics and mechanics together. Often this system of equations is computationally taxing and there is no clear consensus on what set of field equations should be used. In the microfluidics domain stimuli-responsive hydrogels are used as sensors and actuators because of the ease of fabrication and the natural actuation of the material when an external stimulus is supplied.

One of the main issues that surrounds the calculation of the stress field within these hydrogels during the actuation process taking place in microfluidic devices is the fact that these materials undergo swelling. This process makes complicated boundary value

problems even more challenging because of the moving boundaries of the diffusion front and the surface of the swelling hydrogel.

It is important to direct emphasis to the fact that the Fung parameter β° is a measure of the relative nonlinear coupling between stress and strain. This will manifest itself, for a one dimensional tensile test, as a strain hardening or strain softening effect. For the tests conducted on the HEMA-DMAEMA stimuli-responsive hydrogel strain softening was observed. A β° above ≈ 1.1 for HEMA-DMAEMA shows strain hardening. Values between $0 \leq \beta^\circ \leq 1.1$ display varying degrees of strain softening. The value of the Fung parameter β° for HEMA-DMAEMA stimuli-responsive hydrogels is $\beta^\circ = 0.87 \pm 0.018$. This value for β° was tested against experimental tensile testing data and was found to be in good agreement for stretches ranging from 1.0 to 1.4. After λ=1.4 the theoretical prediction gave a lower magnitude for the stress. The coupling from this formulation is shown to have good agreement for moderate strains but does deviate for much larger deformations. In the 1D Fung's law representation the Young's modulus and the Fung parameter are completed separated from one another. In Freed's 3D formulation these two terms are coupled together.

Fung's law is used primarily in the biomechanics community as a method of characterizing soft tissues. A three dimensional analogous strain energy function is introduced here[13] as a general representation for soft materials. Tests have been performed on porcine, mitral-valve chordae tendineae extended in tension[14]. The Fung parameter reported ranged between 7.68 and 9.09 depending on the stress measurement taken[14, 15]. Inferior glenohumeral ligament was also tested in tension and the results were analyzed

using Fung's law[3]. The average Fung parameter reported for the superior, anterior and posterior ligaments was 11.44±4.60. This quantifies substantial strain stiffening. Such stiffening is helpful in the function of ligament. The ligament is compliant over a wide range of motion of the limbs, so there is little resistance to motion. The stiffening at larger strain provides stability of the joint at extremes of the range of motion. Porcine brains were characterized in simple shear at dynamic strain rates and the Fung parameter was reported to range from 0.122±0.022 to 0.229±0.04[28].

In the future, further modification of the implicit constitutive relationship needs to be performed. Equi-biaxial testing should be conducted to confirm the validity of β° in the two dimensional regime. Theoretical framework for interpretation of such tests has been provided in this article. Further down the line β° can be tested in more complex situations and the validity of this implicit formulation can be confirmed.

3.4 Conclusion

In this paper, we measured the Fung parameter β° for HEMA-DMAEMA stimuli-responsive hydrogels. The experimental results indicted that β° yielded a resulting stress-strain curve that matched closely to measured data for stretches 1.4 and below. For stretches above 1.4 the theoretical predictions were slightly lower than the experimental data obstained. The tests were conducted in different pH environments that matched conditions seen in

microfluidic devices. The relative degree of strain hardening and softening can be represented by the Fung parameter β°. This result shows that implicit elastic formulations can be used to model stimuli-responsive hydrogels.

3.5 Acknowledgments

I would like to acknowledge helpful conversations that I have had with Dr. Mehrdad Arjmand, and professor Robert Witt on the conceptual application of implicit elasticity and future numerical methods. Additionally I would like to acknowledge professor David Beebe for use of his lab equipment and space when fabricating samples for testing.

Bibliography

[1] S Baek and AR Srinivasa. Modeling of the ph-sensitive behavior of an ionic gel in the presence of diffusion. *International Journal of Non-linear Mechanics*, 39(8): 1301–1318, 2004.

[2] David J Beebe, Jeffrey S Moore, Joseph M Bauer, Qing Yu, Robin H Liu, Chelladurai Devadoss, and Byung-Ho Jo. Functional hydrogel structures for autonomous flow control inside microfluidic channels. *Nature*, 404(6778):588–590, 2000.

[3] Louis U Bigliani, Roger G Pollock, Louis J Soslowsky, Evan L Flatow, Robert J Pawluk, and Van C Mow. Tensile properties of the inferior glenohumeral ligament. *Journal of Orthopaedic Research*, 10(2):187–197, 1992.

[4] David Brock, Woojin Lee, Daniel Segalman, and Walter Witkowski. A dynamic model of a linear actuator based on polymer hydrogel. *Journal of Intelligent Material Systems and Structures*, 5(6):764–771, 1994.

[5] Xia Cao, Siyi Lai, and L James Lee. Design of a self-regulated drug delivery device. *Biomedical Microdevices*, 3(2):109–118, 2001.

[6] Sudipto K De, NR Aluru, B Johnson, WC Crone, David J Beebe, and J Moore. Equilibrium swelling and kinetics of ph-responsive hydrogels: Models, experiments, and simulations. *Journal of Microelectromechanical Systems*, 11(5):544–555, 2002.

[7] Liang Dong and Hongrui Jiang. Autonomous microfluidics with stimuli-responsive hydrogels. *Soft matter*, 3(10):1223–1230, 2007.

[8] Liang Dong, Abhishek K Agarwal, David J Beebe, and Hongrui Jiang. Adaptive liquid microlenses activated by stimuli-responsive hydrogels. *Nature*, 442(7102):551–554, 2006.

[9] CJ Durning and KN Morman Jr. Nonlinear swelling of polymer gels. *The Journal of chemical physics*, 98(5):4275–4293, 1993.

[10] Fariba Fischel-Ghodsian, Larry Brown, Edith Mathiowitz, Dietrich Brandenburg, and Robert Langer. Enzymatically controlled drug delivery. *Proceedings of the National Academy of Sciences*, 85(7):2403–2406, 1988.

[11] Paul J. Flory. *Principles of polymer chemistry*. Cornell University Press, 1953.

[12] Paul J Flory and John Rehner Jr. Statistical mechanics of cross-linked polymer networks i. rubberlike elasticity. *The Journal of Chemical Physics*, 11(11):512–520, 1943.

[13] Alan D Freed. Soft solids. *Modeling and Simulation in Science, Engineering and Technology (Birkhäuser, Basel, 2014), a Primer to the Theoretical Mechanics of Materials*, 2014.

[14] Alan D Freed and Todd C Doehring. Elastic model for crimped collagen fibrils. *Journal of biomechanical engineering*, 127(4):587–593, 2005.

[15] Alan D Freed and KR Rajagopal. A promising approach for modeling biological fibers. *Acta Mechanica*, 227(6):1609, 2016.

[16] YC Fung. Elasticity of soft tissues in simple elongation. *American Journal of Physiology–Legacy Content*, 213(6):1532–1544, 1967.

[17] Piyush Gupta, Kavita Vermani, and Sanjay Garg. Hydrogels: from controlled release to ph-responsive drug delivery. *Drug discovery today*, 7(10):569–579, 2002.

[18] Kenneth D Harris, Cees WM Bastiaansen, and Dirk J Broer. A glassy bending-mode polymeric actuator which deforms in response to solvent polarity. *Macromolecular rapid communications*, 27(16):1323–1329, 2006.

[19] A Gerhard Holzapfel. Nonlinear solid mechanics ii. 2000.

[20] Wei Hong, Xuanhe Zhao, Jinxiong Zhou, and Zhigang Suo. A theory of coupled diffusion and large deformation in polymeric gels. *Journal of the Mechanics and Physics of Solids*, 56(5):1779–1793, 2008.

[21] Joseph Jagur-Grodzinski. Polymers for tissue engineering, medical devices, and regenerative medicine. concise general review of recent studies. *Polymers for advanced technologies*, 17(6):395–418, 2006.

[22] Hongrui Jiang and Difeng Zhu. Hydrogels as actuators for biological applications. In *GELS HANDBOOK: Fundamentals, Properties and Applications Volume 3: Application of Hydrogels in Drug Delivery and Biosensing*, pages 149–187. World Scientific, 2016.

[23] B.D. Johnson, J.M. Bauer, D.J. Niedermaier, W.C. Crone, and D.J. Beebe. Experimental techniques for mechanical characterization of hydrogels at the microscale. *Experimental Mechanics*, 44(1):21–28, 2004.

[24] A Katchalsky and I Michaeli. Polyelectrolyte gels in salt solutions. *Journal of Polymer Science Part A: Polymer Chemistry*, 15(79):69–86, 1955.

[25] Robert Langer. Drug deliveryand targeting. *Nature*, 392(6679):5–10, 1998.

[26] Mingming Ma, Liang Guo, Daniel G Anderson, and Robert Langer. Bio-inspired polymer composite actuator and generator driven by water gradients. *Science*, 339 (6116):186–189, 2013.

[27] Kumbakonam R Rajagopal. On implicit constitutive theories. *Applications of Mathematics*, 48(4):279–319, 2003.

[28] Badar Rashid, Michel Destrade, and Michael D Gilchrist. Mechanical characterization of brain tissue in simple shear at dynamic strain rates. *Journal of the mechanical behavior of biomedical materials*, 28:71–85, 2013.

[29] Debashish Roy, Jennifer N Cambre, and Brent S Sumerlin. Future perspectives and recent advances in stimuli-responsive materials. *Progress in Polymer Science*, 35(1): 278–301, 2010.

[30] ASTM Standard. D638: Standard test method for tensile properties of plastics. *West Conshohocken (PA): ASTM International*, 2010.

[31] Toyoichi Tanaka and David J Fillmore. Kinetics of swelling of gels. *The Journal of Chemical Physics*, 70(3):1214–1218, 1979.

[32] Leslie Ronald George Treloar. *The physics of rubber elasticity*. Oxford University Press, USA, 1975.

[33] Clifford Truesdell and Walter Noll. The non-linear field theories of mechanics. In *The non-linear field theories of mechanics*, pages 1–579. Springer, 2004.

Chapter 4

Interfacial Adhesion

4.1 Introduction

Microfluidics and microelectromechanical-based devices (MEMS) provide the potential for higher levels of functional integration, increased performance, lower cost advantages, decreased size, and increased reliability, in a wide range of potential applications. There are a number of important properties that make microfluidic systems uniquely attractive: flow is typically laminar, turbulence is not present, diffusion times are short, and the surface to volume ratio is large[15, 19, 29, 42]. Much of the research to date in the area of microfluidics has focused on "lab-on-a-chip" devices and microfluidic systems for drug delivery, however there are a wide range of potential applications such as high-precision pressure regulators, pressure-based mass flow controllers, and low leak-rate shut-off micro-valves appropriate for use in vacuum system applications[2].

A critical material used in many microfluidic device designs is a responsive hydrogel. These materials constitute a class of shape memory materials that are capable of responding to a range of stimuli, and have been successfully used as sensor/actuator components to create autonomous microfluidic devices. Two key features make stimuli-responsive hydrogels attractive for microfluidic devices: the ability to fabricate structures in a fluidic environment by photo-polymerization; and the autonomous nature of their response, providing a method for autonomous sensing and actuation. [5] Stimuli-responsive hydrogels have the ability to respond in a defined manner to a wide range of external stimuli ranging from pH and temperature, to chemical and biological signals, including air/liquid-bourne molecules and contaminants. These materials operate in a hydrated environment and the hydrogel responds with a significant volumetric reversible transformation through absorption or release of solvent within the polymeric network.

Examples of microfluidic systems employing responsive hydrogels include: thermally actuated microlenses[3, 51] autonomously triggered on-chip microfluidic cooling devices[1], adaptive liquid microlenses [11, 28], modular perfusion system for high-resolution microscopes [18], mass-produced valve actuating hydrogels for assembly of commercial microfluidic products [25], inchworm microrobot [23], infusion device for continuous delivery of protein therapeutics [13], hand-held disposable botulinum toxin assay microsystem [32], valved microdispensing device [12], thermoresponsive actuators for lab-on-a-chip devices [31], and autonomously regulated pH systems [14].

Microfluidic design and device development is often conducted with limited input on the mechanical capabilities of the materials, including the hydrogel materials used in

sensor/actuator components. As the field moves beyond the proof-of-concept devices, more control over the materials design and fundamental understanding of the materials properties is required. In actuation applications, for example, the gels must endure forces imposed by flow of an aqueous solution, the constraint of device walls during swelling, and the restoring force of elastic membranes. [13, 14]

Interfacial adhesion, the focus of this study, plays a critical role in microfludic device applications. Fot instance, those that require optimum cell adhesion[7, 21], biomimetic hydrogel values[50], and attachment to polydimethylsiloxane substrates[8], in addition to many others.

There are several established methods of interfacial and surface adhesion characterization. One of the most popular adhesive characterization methods is the peel test, this method is used most commonly in the characterization of thin films on substrates[10]. For this test tape (thin film) is bonded to a rigid substrate via an adhesive that is to be tested. The thin film is then pulled apart from the substrate at a constant rate and angle. A plot of the force versus grip separation is compiled and the average peel force is then calculated.

When this test is performed the region of interest is subjected to mode I and mode II loading. The *mode mixity* is the ratio of these two loadings. This becomes important because many types of adhesive are sensitive to the mode mixity.

The peel test does have many advantages. In general the samples are easy to prepare and test. The peel test will give a quasi-quantitative measure of adhesion strength. This

gives an experimenter an easy method of ranking the strengths of different adhesives. The geometry of deformation creates a stress concentration at the point of delamination. Additionally the rate of strain is a controlled parameter and this dependence can be measured.

The peel test does have drawbacks. Geometry can be a draw back when trying to relate results of experimentation to actual loading conditions. High strains induced at the point of delamination are quite often not experienced in real applications.

The peel test has a disadvantage in which it can only test materials on flexible coatings the pull test has an applicability to a brittle coatings as well. In the pull test one applied a load to both samples and pulls them apart in shear or in tension. This test will garner qualitative and semi-qualitative results and like the peel test the test specimens are generally easy to prepare. Some of the issues associated with this test are the fact that off-axis loading can occur that induces moments in the coatings. No sample coating can be completely bonded to a substrate. Because of this, the pull test will always debond first at the point of any defects in the coating. The difficulty in loading a sample in pure tension can bring about mode mixity. This mode mixity is difficult to measure and can cause a great deal of variability in the test results[26, 47].

Despite these drawbacks to the pull test is has found a wide range of applications. Saubestre et. al,[41] used the pull method to test the adhesion of electrodeposits to plastics. Jacobsson[22] used several adhesion measurement methods, including the pull test, to

measure the adhesion of thin films. More recently the pull test was used by Pawel and McHargue[35] to measure the adhesion of iron films to sapphire substrates.

Another frequently used method for determination of adhesion characteristics is the blister test. This method is used to test adhesion between a substrate and a flexible layer adhered to the surface. This is done by creating and expanding a blister between the flexible layer and a substrate through a hole in the substrate of pre-determined dimensions[46, 49]. The strain energy release rate ($\mathscr{G}$) is determined by measuring the pressure exerted to create the blister and the radius of curvature of the blister itself. The adhesive surface energy is then backed out from this expression[44].

Some of the first applications of the blister tests were performed by Napolitano et. al.[33, 34], and Dillard et. al.[9, 30]. The blister test has the advantage of giving fully quantitative analysis using methods from fracture mechanics. Because this test can be performed at low strains it does not have the disadvantages inherent in the peel. The biggest drawback to the blister test is that the sample preparation in complicated. When quantitative data is needed for the analysis of adhesion the blister test is one of the best tests available.

The peel, pull, and blister tests cannot be used to determine interfacial adhesion energy for the microfluidic system being tested. Hydrogels need to be hydrated over the course of the experiment. Application of load to initiate the fracture process that delaminates two surfaces cannot be applied at the micro scale in a reliable manner that can easily be

quantified. A method of measuring interfacial adhesion *in-situ* that can supply a driving force for delamination is required.

HEMA-DMAEMA hydrogels have a unique feature in that the process that initiate swelling in the hydrogel also initiates internal forces in the gel. The work to initiate and propagate delamination is developed through the swelling of the hydrogel itself. In this study a test method that takes advantage of this feature of stimuli-responsive hydrogels and measures changes in dimensions and forces produced by the hydrogel during the swelling process is shown. We seek to use energy methods from fracture mechanics to measure the adhesion energy of an interface between a stimuli-responsive polymer 2-hydroxyethyl methacrylate (2 - dimethylamino) ethyl methacrylate (HEMA-DMAEMA) and different substrates using a unique experimental set-up. The results from these experiments can be used by microfluidic device designers.

4.2 Background

There are many adhesion measuring methods that use concepts from fracture mechanics. One of the most popular ones is the double cantilever beam bending test. Some of the more effective methods have their foundations in the Griffith theory of fracture. In 1921 Alan Griffiths introduced his theory of fracture mechanics[20]. When a body transitions from a non-equilibrium state to an equilibrium state according to the First Law of Thermodynamics there has to be a net decrease in energy. Griffith proposed that when forces are applied to a body a crack can only be initiated or an existing crack

can only grow if there is a decrease in the total energy of the body or the total energy remains constant. This theory gives a critical condition under which a crack can be initiated. When the change in the total energy of a body with respect to newly formed surfaces is zero the critical condition for crack growth has been met. This condition can be written as,

$$\frac{dE}{dA} = \frac{dW}{dA} + \frac{dU}{dA} = 0, \tag{4.1}$$

where E it the total energy of the body, W is the work done to create new surfaces, U is the total potential energy of the system minus work done by external forces and A is the newly created surface area. This condition is normally written as,

$$-\frac{dU}{dA} = \frac{dW}{dA} \tag{4.2}$$

and in the fracture mechanics community each side of equation (4.2) is given a special name. The change in potential energy with respect to crack area is called the *strain energy release rate* and the symbol used for it is $\mathscr{G}$. The change in work with respect to crack area is called the *crack resistance* and is usually denoted by the symbol $\mathscr{R}$. Crack growth occurs when the strain energy release rate is greater than or equal to the crack resistance,

$$\mathscr{G} \geq \mathscr{R}. \tag{4.3}$$

Griffith considered the crack resistance to be a constant, $\mathscr{R} = 2\gamma$, where γ is the surface energy of the new surfaces. Theories of adhesion that measure the surface energy use many different techniques to calculate the strain energy release rate, $\mathscr{G}$, in terms of engineering parameters that can be measured and back out the surface energy term from these calculations. The strain energy release rate is related to the strain energy and the work done by external forces,

$$\mathscr{G} = \frac{\partial(U - F)}{\partial A} \tag{4.4}$$

where F is the work done by external forces, U is the strain potential energy and A is the crack area. The strain energy U can be expressed in terms of the strain energy density $\mathscr{W}$,

$$\frac{dU}{dV} = \mathscr{W}, \tag{4.5}$$

where V is the volume of the body. Using this relationship the strain energy release rate can be determined by,

$$\mathscr{G} = \frac{dU}{dV}\frac{dV}{dA} = \mathscr{W}\frac{dV}{dA}. \tag{4.6}$$

Determination of the strain energy release rate by this process assumes that there is

no external work being done by applied tractions. The stimuli-responsive hydrogel 2-hydroxyethyl methacrylate (HEMA) dimethlaminoethyl methacrylate (DMAEMA) is being studied in this paper and responds specifically to an external diffusing buffer solution of an acidic pH. HEMA-DMAEMA will swell based on the electrostatic repulsion of the bound charges of the polymer chains.[16, 27, 36] The experiments conducted in this paper look to calculate the interfacial adhesion energy between the HEMA-DMAEMA hydrogel and different substrates using equation 4.6 based upon Griffiths fracture theory.

HEMA-DMAEMA stimuli-responsive hydrogels can be considered to behave like an implicit elastic material[37, 38]. For implicit elastic materials stress is not an explicit function of only the current state of stress in a body but instead is a function of the history of stress and strain in a body. HEMA-DMAEMA is a stimuli-responsive hydrogel that can have a state of stress induced inside the body of the hydrogel by diffusion of ionic solutions. When H^+ diffuses into the hydrogel it reacts with OH^- loosely bonded to the cross-linked polymer chains. This process creates H_2O in the gel and causes the gel to swell. There is an increase in osmotic and hydrostatic pressure inside the hydrogel because of these chemical reactions. The spatial distributions of these reactions is diffusion dependent and are thereby geometry dependent. The stress state of these materials does depend boundary conditions and thus the history of stress, and strain, in the body determines its current stress state. Stimuli-responsive hydrogels are in general 95% to 99% water in content and are considered incompressible materials. From this assumption the Poisson ratio of these materials is taken to be $\nu = 1/2$. For incompressible soft materials the complete state of stress, regardless of the deformation history is determined not only

by the constitutive relationships but also by the boundary conditions of the problem. The complete stress state thus takes the form,

$$\mathbf{\Pi} = \mathbf{S} + p\mathbf{C^{-1}}, \tag{4.7}$$

where $\mathbf{S}$ is the 2nd Piola-Kirchoff stress, $\mathbf{C}$ is the Cauchy deformation tensor defined as $\mathbf{C} = \mathbf{F^T F}$, $\mathbf{F}$ is the deformation gradient, p is a Lagrange multiplier that in analogous to a hydrostatic pressure term and $\mathbf{\Pi}$ is called the *extra stress*[17, 43]. The implicit form of the strain energy is given as,

$$\mathscr{W}(E, \Pi; C) = \frac{-\nu}{2E_a} tr^2(\mathbf{\Pi C}) + \frac{1+\nu}{2E_a} tr(\mathbf{\Pi C \Pi C}) - \frac{\beta^\circ}{2E_a} tr(\mathbf{\Pi E \Pi C}), \tag{4.8}$$

where $\mathbf{E}$ is Green strain given by $\mathbf{E} = (1/2)(\mathbf{C} - \mathbf{I})$, $\mathbf{I}$ is the identity tensor, ν is the Poisson ratio that is assumed to be $1/2$ for incompressible materials, and E_a is an assumed Young's modulus. The assumed Young's modulus is taken to be equal to $E_a = 3G$ for incompressible materials the shear modulus G is the shear modulus determined from uniaxial tension tests using the relationship from rubber elasticity theory[45] $\sigma = G(\lambda - \lambda^{-2})$ where λ is the defined as the stretch which is final length over initial length. The term $(\lambda - \lambda^{-2})$ is referred to as the modified stretch. The constitutive equation for implicit elastic solids can be written as[**?**],

$$\mathbf{dS} = \mathbf{M} \cdot \cdot \mathbf{dE}, \tag{4.9}$$

Where the tensor that contracts stress with strain $\mathbf{M}$ is the Tangent Modulus and $(\cdot\cdot)$ is a outer double dot product defined as, $(\mathbf{M}\cdot\cdot\mathbf{N} = M_{ij}N_{ij})$. Implicit elasticity theory gives stress rate and a function of strain rate.

4.3 Methods

A prepolymer solution is prepared using the reagents, 2-(dimethylamino) ethyl methacrylate (DMAEMA), 2-hydroxyethl methacrylate (HEMA), ethylene glycol dimethacrylate (EGDMA) and 2,2-dimethoxy-2-phenylacetophenone (DMPA). The reagents are mixed together in the following ratios, 25.77:5.718:0.467:1. All reagents were purchased from Sigma-Aldrich. Prior to polymerization this hydrogel-liquid solution is stored at $-8°$C.

Using the *in situ* photo-polymerization techniques developed for the creation of hydrogel actuators in microfluidic devices as a starting point, the procedure was modified to create the test samples for the experiments described below[24]. First a suitable substrate is mounted in a standard petri dish. A steel spacer is placed on top of the substrate that has a well in the middle to contain the pre-polymer solution as shown in part a.) of figure 4.1. The hydrogel-liquid solution described above is placed in the well via pipette. The well is shown schematically in part c.) of figure 4.1 and the spacer has a thickness of 0.3 mm. The spacer is made out of stainless steel and has the width of a standard glass slide.

Hydrogel samples are prepared on 3 different substrates. Premium fully frosted borosilicate glass slides modified by surface sand blasting, 12-544-5CY, clear borosilicate glass

slides coated with polysine adhesive, 12-545-78 and plain borosilicate glass slides pre-cleaned, 12-544-1. All slides were purchased from Fisher Scientific.

Samples are pre-conditioned in 7.0 pH de-ionized water for a period of twenty-four hours. During the tests the hydrogel is swollen in 3.0 pH buffer solution for a duration of 120 minutes. During swelling images are taken every 30 seconds using a 45^0 mirror mounted below the substrate as shown in figure 4.3. A Q-Imaging MicroPublisher 5.0 RTV camera with an Optem Zoom 200 lens is used to record sample images during the test. QCapture Pro software is used to record the image stacks.

A colorless DuPont Tenjin Film is used as a plastic cover slip and is placed over top of the steel spacer and hydrogel-liquid solution to provide an easily removable seal to the top of the well. A mask printed with the desired features is then placed on top of the colorless plastic cover slip as shown in part b.) of figure 4.1. Polymerization is achieved by exposing the hydrogel-liquid solution to UV light at an intensity of 20mW/cm^2 for a total time of 49.0 seconds. One the cylindrical posts have been polymerized the mask is first removed then the colorless plastic cover slip. Before the plastic cover slip is removed from the well the edges where the cover slip and the spacer should be separated. This was done using a simple razor blade. It was found that this separation needed to take place otherwise to much force was required to remove the cover slip from the spacer and this would cause the hydrogel posts to adhere to the cover slip and not the substrate. The UV-polymerization is done with an EFOS Acticure A4000 UV Spot Curing System. When the polymerization is complete, the mask is removed, followed by the colorless film. An ethanol rinse (pH 7.0) is used on the resultant polymer to remove any excess solution.

For this experiment, these hydrogels were fabricated in the form of six cylindrical posts. The radii of the fabricated cylindrical posts are 300 μm, 350 μm and 400 μm and the heights of the posts are $\approx 300\mu m$.

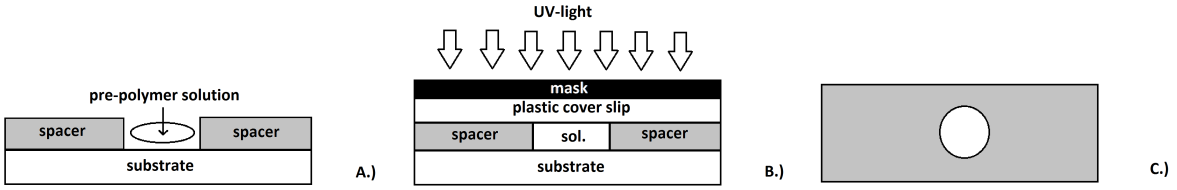

FIGURE 4.1: Part A.) represent a side view of the experimental setup. A glass microscope slide represents the substrate and a metal spacer is placed on top of the substrate with a well in the middle. In the well the pre polymer solution is placed. In part B.) shows the set up after the pre polymer solution is added, a transparent plastic cover slip is placed on top of the metal spacer and then the desired mask is placed on top of the cover slip. Part C.) is the top down view of the metal spacer.

One custom acrylic compression platen is used during testing. When the samples are mounted in the petri dish as shown in 4.3 the compression platen is brought to within 300 μm from the substrate which is the fabricated height of the hydrogels. The compression platen is then lowered 20 μm into the hydrogel to begin testing. There is a period of 20 seconds that elapses before the external buffer is added to the petri dish and swelling begins. The swelling test runs for a two hour period of time.

In figure 4.2 a schematic of the delamination process is shown. They hydrogel will start out the process completely attached to the substrate. As the external aqueous buffer solution is introduced the gel expands and delamination occurs. The delamination front propagates inwards during swelling and remains circular throughout the fracture process.

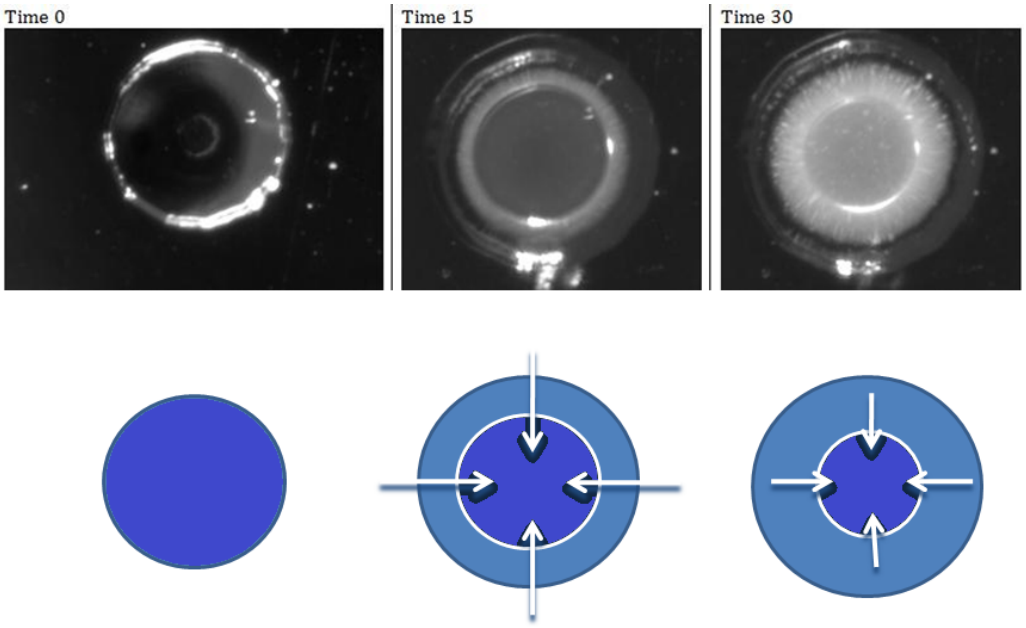

FIGURE 4.2: Schematic of the delamination process. Going from left to right the hydrogel delaminates inwards while the gel expands outwards over time.

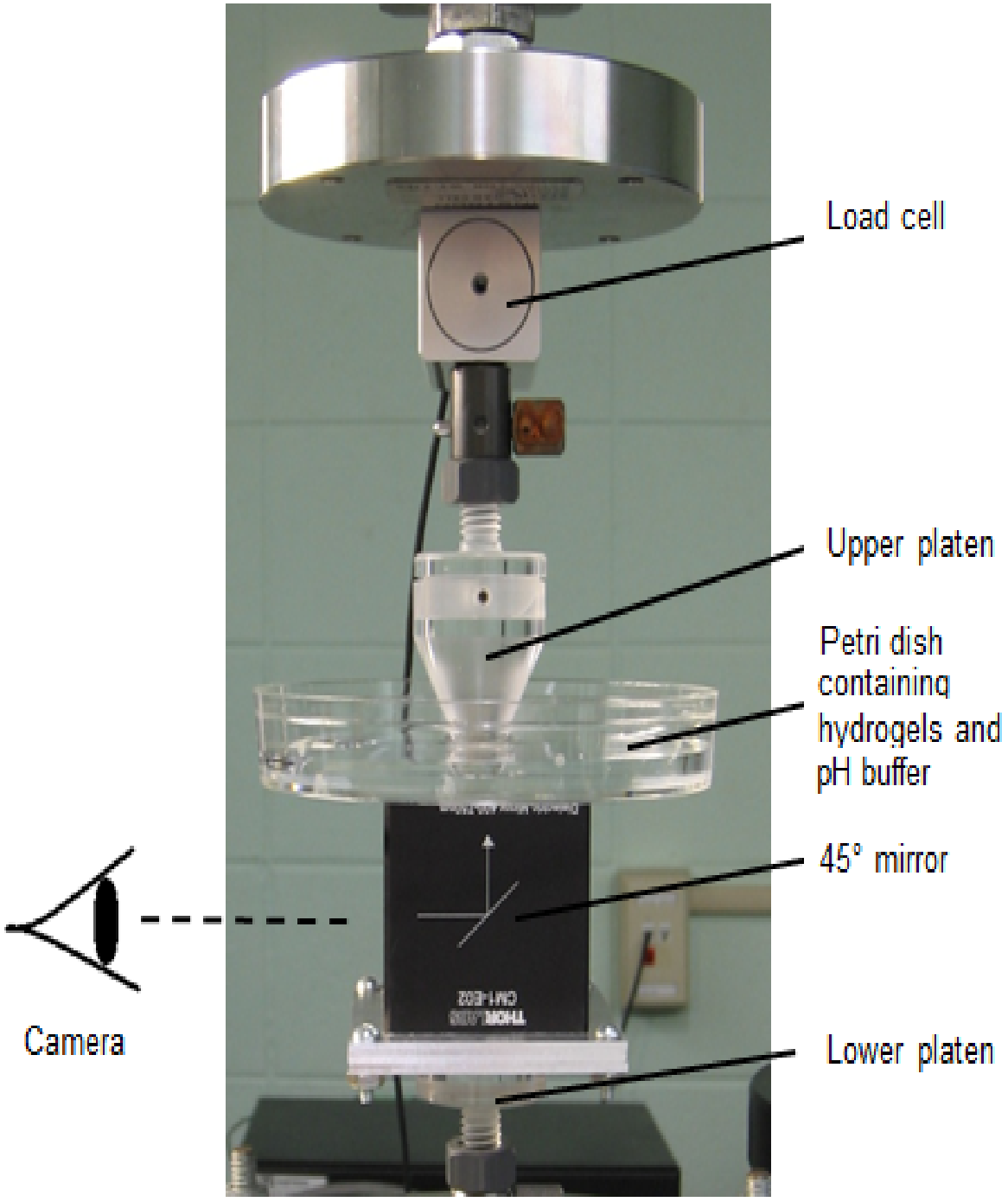

FIGURE 4.3: Hydrogel Experimental Set-up. The upper platen of the micro Instron is lowered to height of the hydrogel samples and constrains them from swelling in the axial direction. A 45° mirror is mounted below the samples and camera is located, off screen, that images the hydrogels during expansion[6].

To determine the interfacial adhesion energy the point at which the strain energy release rate $\mathscr{G}$ is equal to the crack resistance $\mathscr{R}$ is used. This relationship is given as,

$$\frac{\mathscr{G}}{2} = \gamma, \tag{4.10}$$

where γ is the surface energy term. From equation (4.6) the term dV/dA is easily obtained for cylindrical geometry. The volume of a cylinder is simply $V = Ah$ were h is the height of the cylinder. Thus $dV/dA = h$ and the surface energy term is,

$$\gamma = \mathscr{W}\frac{h}{2}, \tag{4.11}$$

and all that is left is the calculation of the strain energy $\mathscr{W}$. From this experimental set up we measure the axial load, the radial stretch and the crack velocity. The radial stretch λ and the axial load are used to determine the interfacial surface energy of the hydrogel on modified borosilicate glass substrates. The crack velocity is shown to be faster on substrates with poor adhesion. This measurement of crack velocity is used as a visual characterization of surface adhesion that should coincide with the measurements of interfacial adhesion energy.

To describe the kinematics of the problem the deformation gradient $\mathbf{F}$ must be defined. In order to accomplish this we can take advantage of the fact that the ratio of final to initial volumes of a material is known as the determinate of the deformation gradient $\mathbf{F}$. The hydrogel is constrained axially in this experiment and is only allowed to expand

radially. This motion of the hydrogel is assume to occur only in the principle directions and from axial symmetry and the axial constraint of the hydrogel forces displacements in only in the radial direction. Using the relationship,

$$det(\mathbf{F}) = \lambda_r \lambda_\theta \lambda_z = \frac{V_f}{V_i} = \frac{\pi(\lambda_r^2 r^2)}{\pi r^2} = \lambda_r^2. \tag{4.12}$$

From equation (A.4) it is shown that $\lambda_\theta \lambda_z = \lambda_r$. Given that the material is constrained axially and $\lambda_z = 1$, $\lambda_\theta = \lambda_r$ and thus, dropping the subscrip r we can write the deformation gradient as, $\mathbf{F} = diag(\lambda, \lambda, 1)$.

With this definition of the deformation gradient $\mathbf{F}$, and the assumption of incompressibility, (ν=1/2).

For implicit elastic materials stress is now an implicit function of stress and strain. The strain energy function that stresses are derived from takes on the form, $\mathscr{W}(\mathbf{E}, \mathbf{\Pi}; \mathbf{C})$ where the potential function is now expressed in term of the history of stress in the material. The Tangent modulus from equation (4.9) contracts strain rate with stress rate and is determined from the following formulation,

$$\mathbf{M} = \left(\frac{\partial^2 W}{\partial \mathbf{\Pi} \partial \mathbf{\Pi}} \right)^{-1} : \left(\mathbf{I} - \frac{\partial^2 W}{\partial \mathbf{\Pi} \partial \mathbf{E}} \right), \tag{4.13}$$

where the inner double dot (:) is defined as, $M : N = M_{ij} N_{ji}$. The main difference between the Tangent modulus and the Elasticity tensor common in elasticity theory is

that the components of the Tangent modulus can themselves be functions of stress and strain. For the Elasticity tensor all of its components are constant valued. Using the deformation gradient defined above and taking the partial derivatives of equation (4.8) the Tangent modulus is given as,

$$\mathbf{M} = \begin{pmatrix} -\frac{\left(\Pi_{11}\beta^\circ\lambda^2+E_a\right)\left((2\beta^\circ-3)\lambda^2-2\beta^\circ\right)}{\beta^\circ\lambda^2(\lambda^2-1)((\beta^\circ-3)\lambda^2-\beta^\circ)} & \frac{3\left(\Pi_{22}\beta^\circ\lambda^2+E_a\right)}{\beta^\circ(\lambda^2-1)((\beta^\circ-3)\lambda^2-\beta^\circ)} & \frac{E_a+\Pi_{33}\beta^\circ}{\beta-\beta^\circ\lambda^2} \\ \frac{3\left(\Pi_{11}\beta^\circ\lambda^2+E_a\right)}{\beta^\circ(\lambda^2-1)((\beta^\circ-3)\lambda^2-\beta^\circ)} & -\frac{\left(\Pi_{22}\beta^\circ\lambda^2+E_a\right)\left((2\beta^\circ-3)\lambda^2-2\beta^\circ\right)}{\beta\lambda^2(\lambda^2-1)((\beta^\circ-3)\lambda^2-\beta^\circ)} & \frac{E_a+\Pi_{33}\beta^\circ}{\beta^\circ-\beta^\circ\lambda^2} \\ \frac{S_{11}\beta^\circ\lambda^2+E_a}{\beta^\circ-\beta^\circ\lambda^2} & \frac{\Pi_{22}\beta^\circ\lambda^2+E_a}{\beta^\circ-\beta^\circ\lambda^2} & \frac{(E_a+\Pi_{33}\beta^\circ)\left((\beta^\circ-1)\lambda^2-\beta^\circ\right)}{\beta^\circ(\lambda^2-1)} \end{pmatrix} \tag{4.14}$$

Equation (4.14) is used in equation (4.9) to determine the stresses. These stresses are then used in equation (4.8) to determine the strain energy. Principle extra stresses Π_{11} and Π_{22} are determined from the measured value of Π_{33}. Radial measurements of the hydrogel during swelling give the values of the stretch λ. Once the strain energy term is calculated it is used in equation (4.10) to calculate the interfacial adhesion energy via,

$$= \frac{(\beta^\circ + (\beta^\circ - 1)\lambda^2)(2E_a dE + S_{33}\beta^\circ(\lambda^2 - 1))^2 h}{16E_a dE^2\beta^{\circ 2}\lambda^2}, \tag{4.15}$$

where h is the height of the hydrogel samples. In this formulation $\beta^\circ = 0.870$ and $E_a = 108kPa$ both values have been determined experimentally for this material from tensile testing. The stretch λ and prior stress Π_{33} are also determined from experimental data.

4.4 Results

A representative plot of the radial stretch is shown for the polysine slides with the 600 μm diameter samples. The buffer solution is introduced to the hydrogel at point A. From points B to D in figure 4.4 the hydrogel is delaminating and the total length of time is represented by C. Point F represents the end of the process when all swelling has taken place.

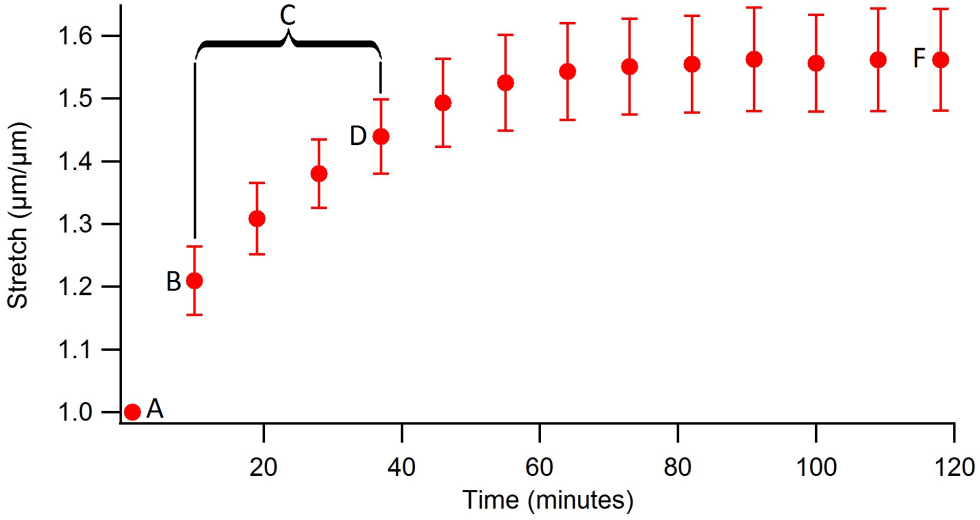

FIGURE 4.4: A representative plot of the radial stretch for the polysine substrate with the 300 μm radius samples. A.) represents the initiation of the swelling, C.) represents the entire range of steady delamination with B.) and D.) representing the beginning and end points of interest and F.) represents the end of swelling.

Observations of the delamination process showed that the hydrogel samples would take longer to delaminate on the larger sample sizes. Within experimental error the crack velocity for the smaller sample sizes are faster than the crack velocity on the larger samples. Figure 4.5 shows the average crack velocity for the 400 μm, 350 μm and 300 μm radius HEMA-DMAEMA samples polymerized on the frosted, plain and polysine

substrates. The crack velocities are shown in nm/s. The crack advances linearly as the diameter of the hydrogel expands in an exponential manner coming to an equilibrium radius.

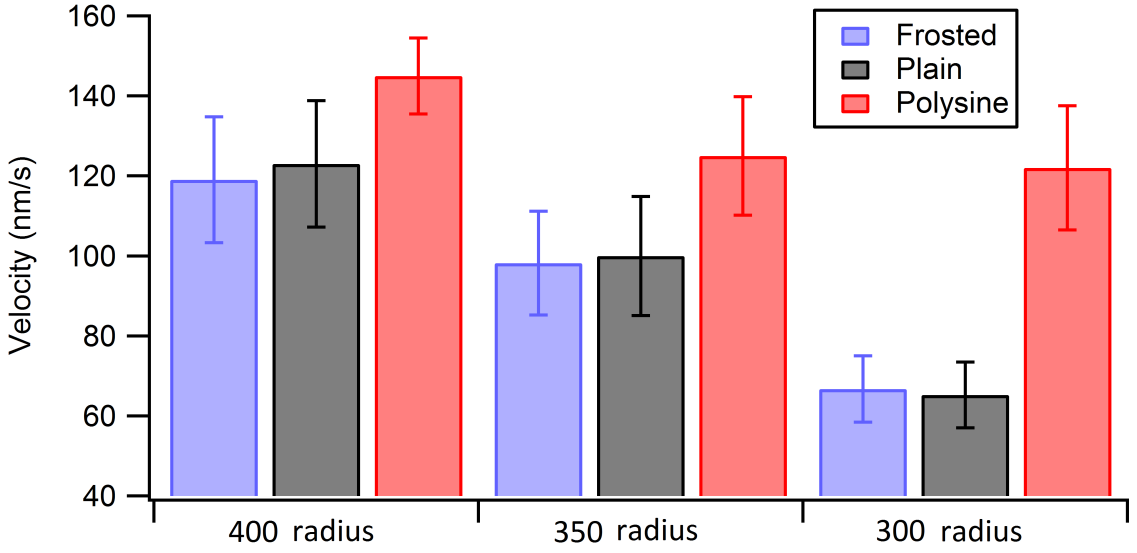

FIGURE 4.5: This bar plot displays the crack velocity during the delamination process on the frosted, plain and polysine substrates.

Crack Velocity nm/sec			
Radius μm	Frosted	Plain	Polysine
300	120±16	120±16	150±9.5
350	98±13	100±15	130±15
400	67±8.3	65±8.2	120±16

TABLE 4.1: Crack velocities in units of nanometers per second.

Plots in figures 4.6 through 4.14 display the radial stretch plotted with the axial stress for each substrate and post size tested. The recorded stresses show a similar pattern

of the stress being larger for the larger substrates and much diminished on the smaller substrates. Figure 4.15 shows the recorded stress at the two-thousand second time point. The error bars are given for the average of all tests recorded at that time point. The values for the recorded stresses is reported in table 4.2. The axial stress is calculated by dividing the load recorded by the Instron by the cross-sectional area and divided by the number of post samples. The cross-sectional area is adjusted to account for the expansion of the hydrogel posts based on the radial stretch that is measured.

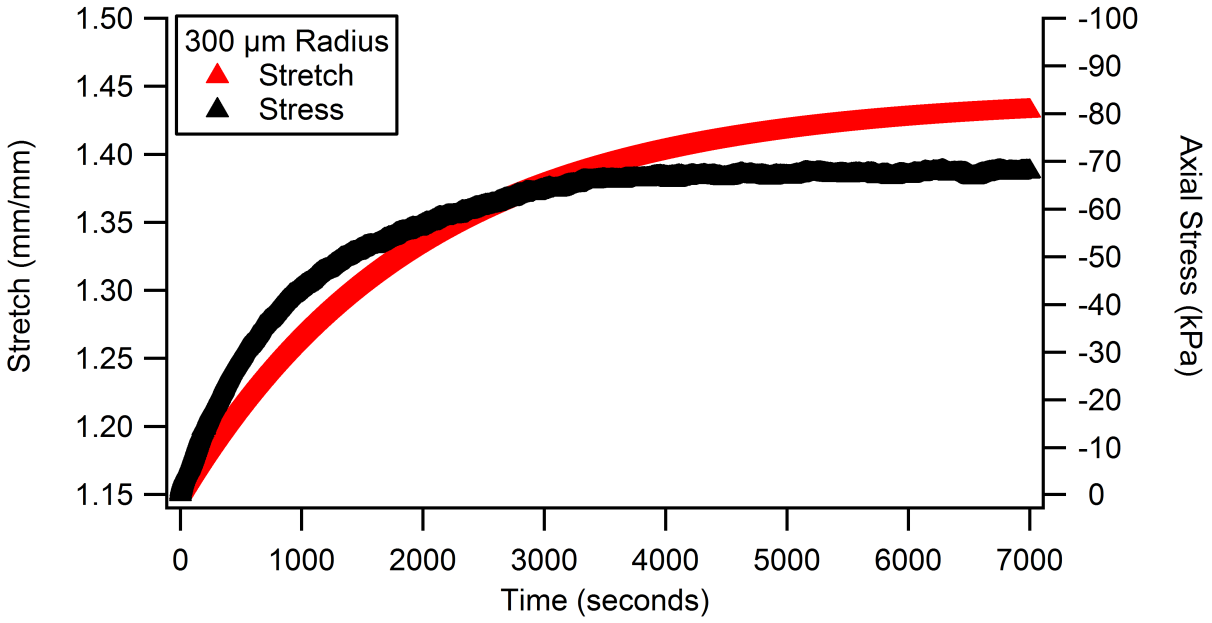

FIGURE 4.6: Axial stress and radial stretch plotted for HEMA-DMAEMA stimuli-responsive hydrogels polymerized on frosted borosilicate glass substrates. The sample size is 300 μm radius cylinder posts that are 300 μm in height.

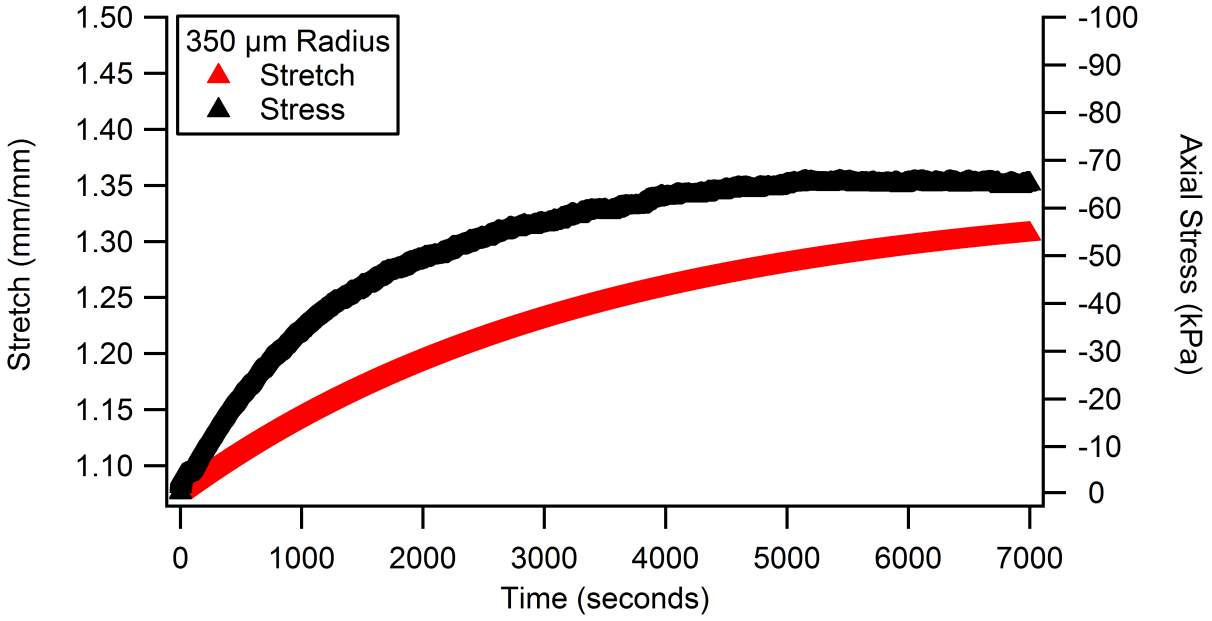

FIGURE 4.7: Axial stress and radial stretch plotted for HEMA-DMAEMA stimuli-responsive hydrogels polymerized on frosted borosilicate glass substrates. The sample size is 350 μm radius cylinder posts that are 300 μm in height.

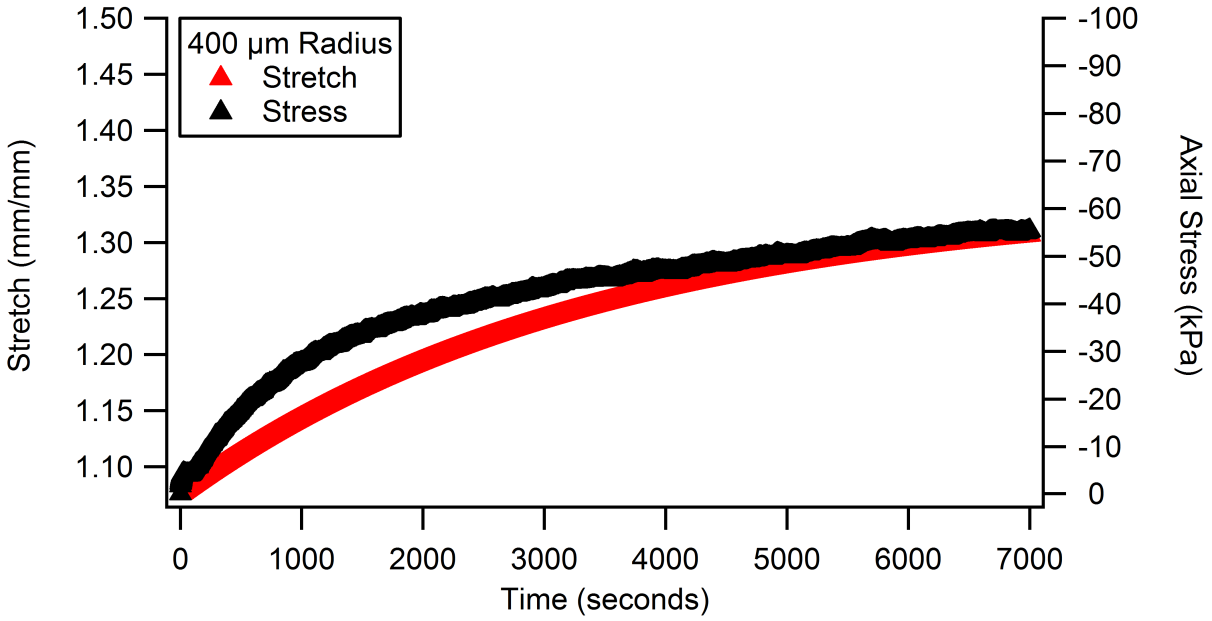

FIGURE 4.8: Axial stress and radial stretch plotted for HEMA-DMAEMA stimuli-responsive hydrogels polymerized on frosted borosilicate glass substrates. The sample size is 400 μm radius cylinder posts that are 300 μm in height.

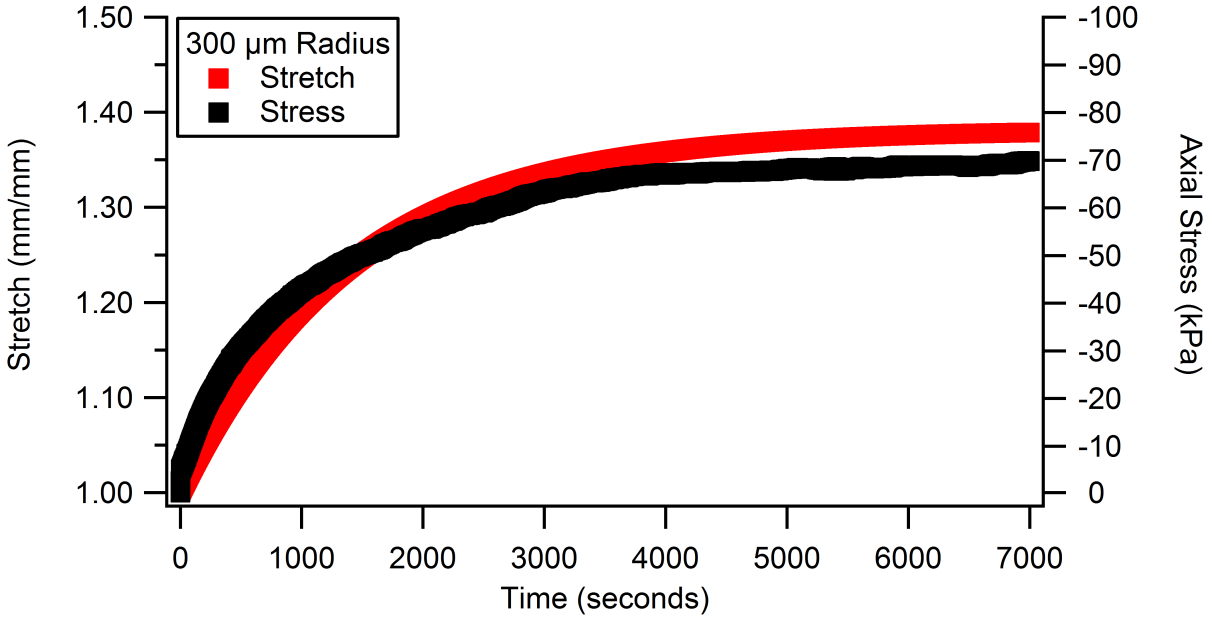

FIGURE 4.9: Axial stress and radial stretch plotted for HEMA-DMAEMA stimuli-responsive hydrogels polymerized on plain borosilicate glass substrates. The sample size is 300 μm radius cylinder posts that are 300 μm in height.

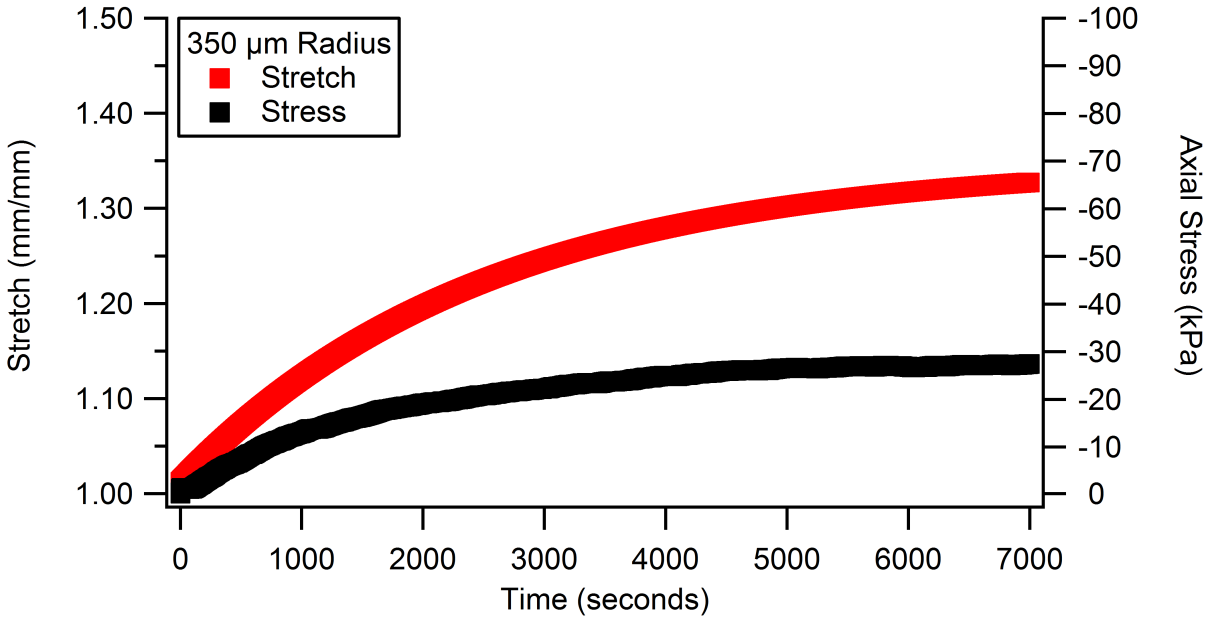

FIGURE 4.10: Axial stress and radial stretch plotted for HEMA-DMAEMA stimuli-responsive hydrogels polymerized on plain borosilicate glass substrates. The sample size is 350 μm radius cylinder posts that are 300 μm in height.

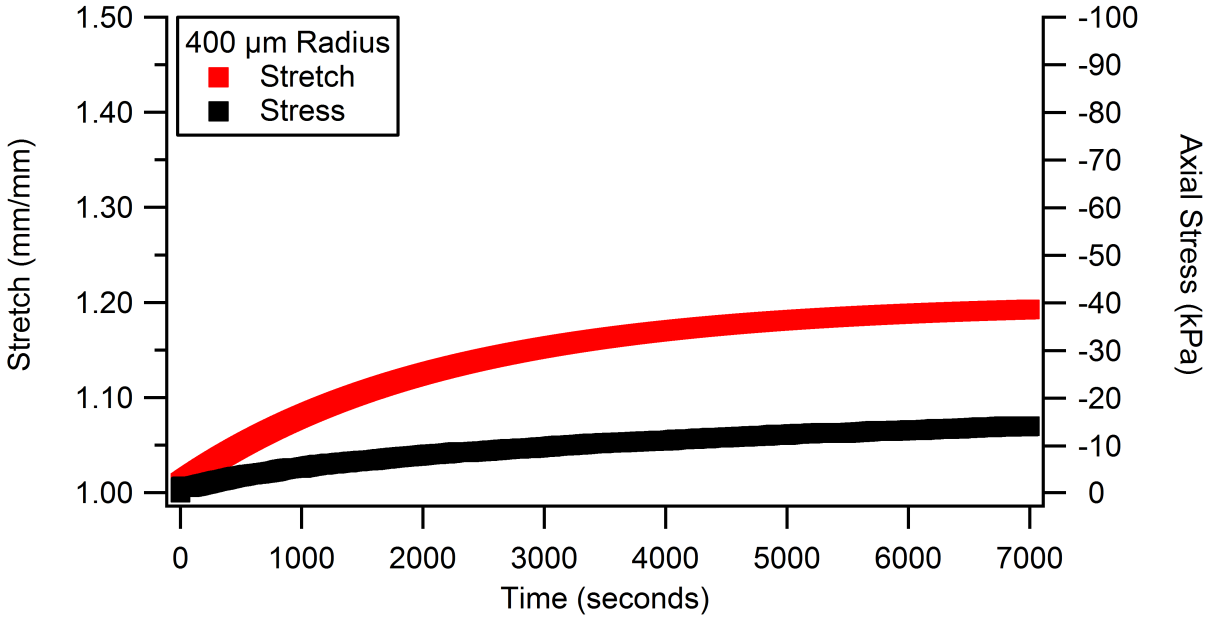

FIGURE 4.11: Axial stress and radial stretch plotted for HEMA-DMAEMA stimuli-responsive hydrogels polymerized on plain borosilicate glass substrates. The sample size is 400 μm radius cylinder posts that are 300 μm in height.

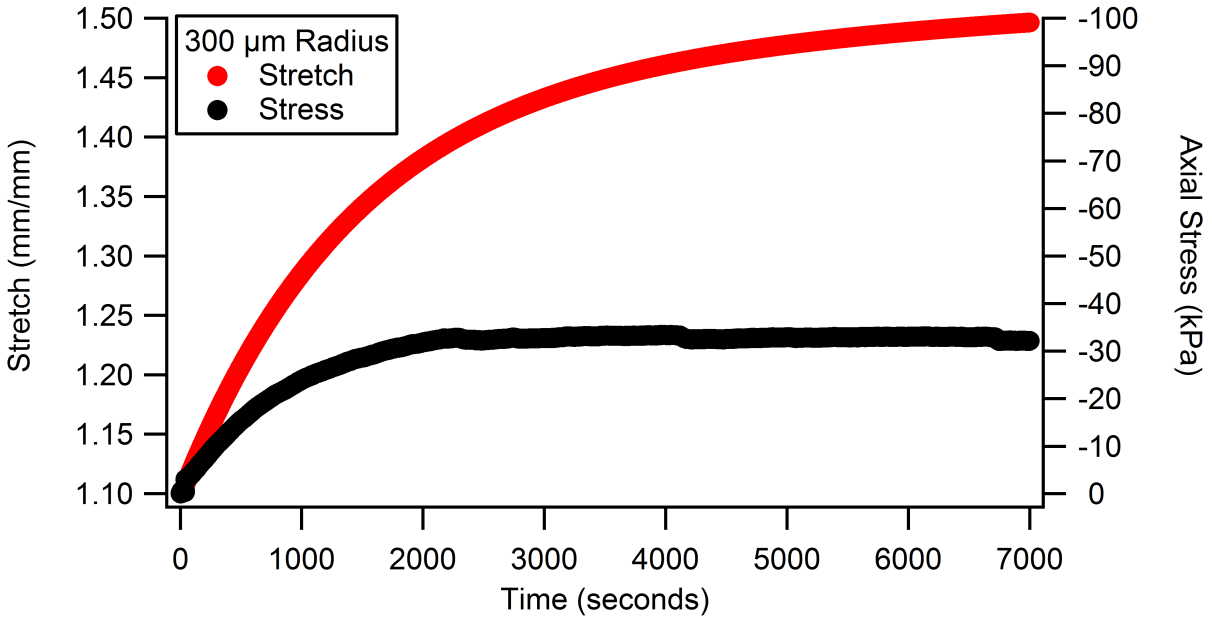

FIGURE 4.12: Axial stress and radial stretch plotted for HEMA-DMAEMA stimuli-responsive hydrogels polymerized on polysine coated borosilicate glass substrates. The sample size is 300 μm radius cylinder posts that are 300 μm in height.

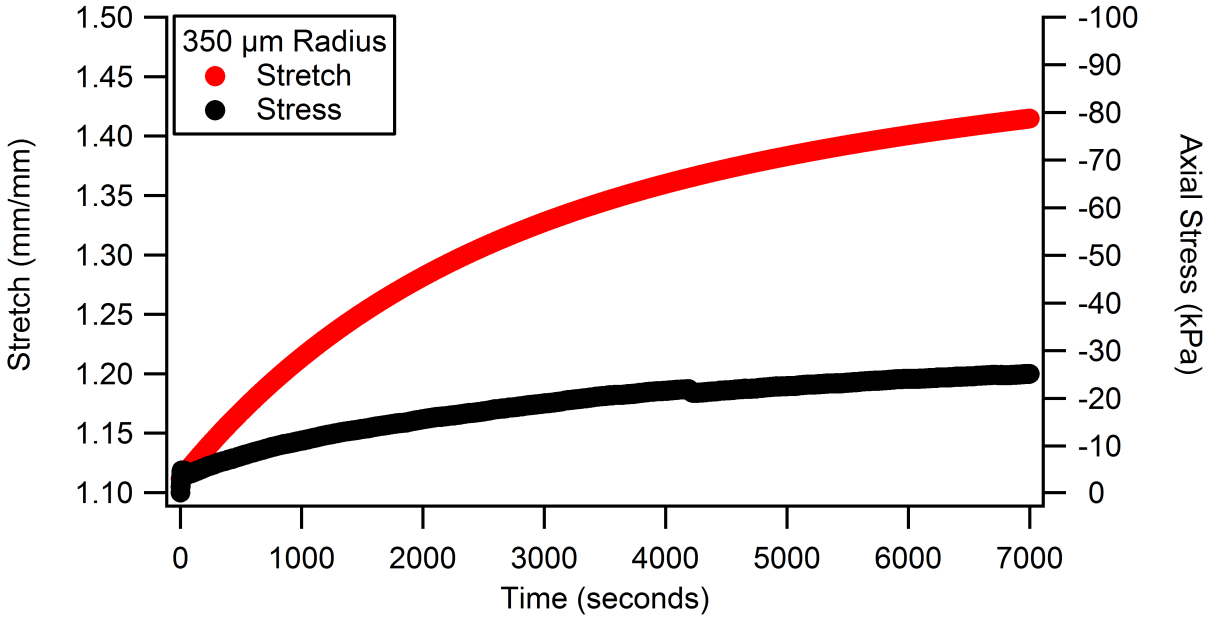

FIGURE 4.13: Axial stress and radial stretch plotted for HEMA-DMAEMA stimuli-responsive hydrogels polymerized on polysine coated borosilicate glass substrates. The sample size is 350 μm radius cylinder posts that are 300 μm in height.

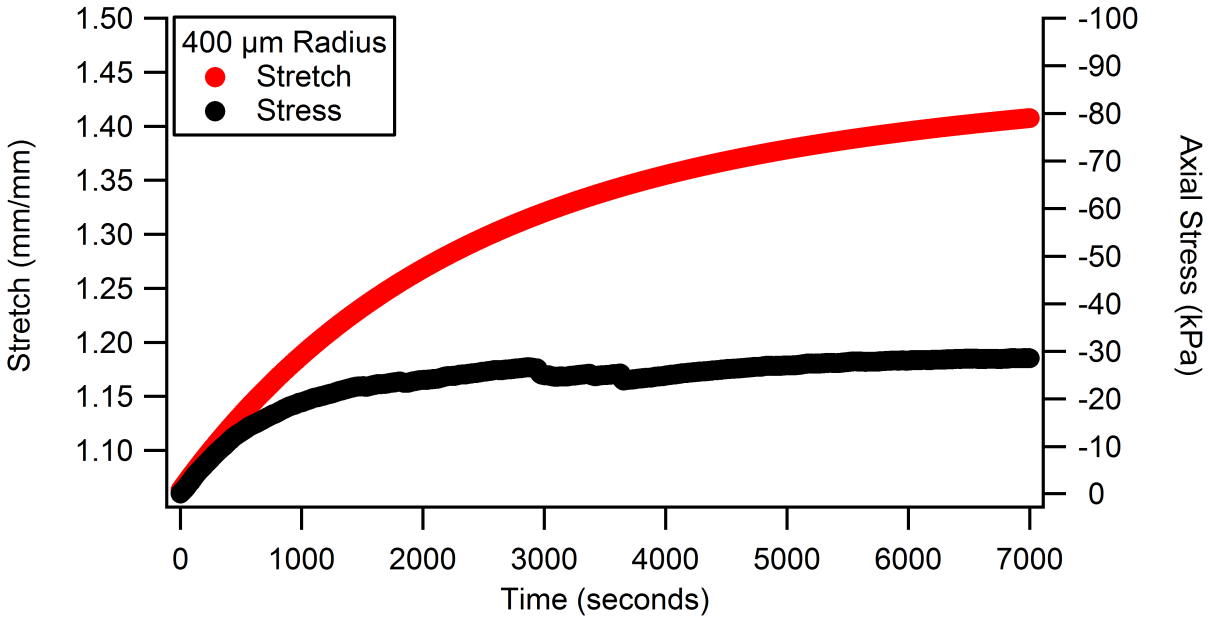

FIGURE 4.14: Axial stress and radial stretch plotted for HEMA-DMAEMA stimuli-responsive hydrogels polymerized on polysine coated borosilicate glass substrates. The sample size is 400 μm radius cylinder posts that are 300 μm in height.

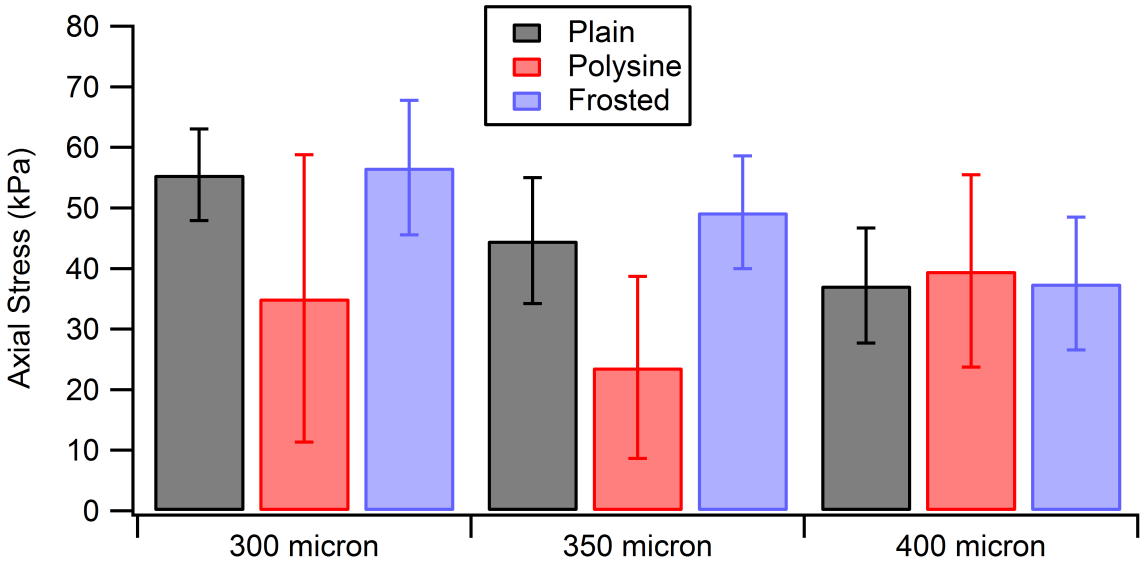

FIGURE 4.15: A bar plot of the stress for each radius and substrate at the 2000 second mark. Bar plot shows the standard deviations of the recorded stress at that time point.

Axial Stress (kPa)			
Radius μm	Plain	Polysine	Frosted
300	55±7.6(18)	35±24(23)	57±11(24)
350	45±10(24)	24±15(20)	49±9.3(24)
400	37±9.5(24)	40±16(16)	38±11(24)

TABLE 4.2: Axial stress recorded at the two-thousand second time point. The number of samples tested for each substrate is given in parenthesis.

Figure 4.16 shows the interfacial adhesion energy of the three substrates tested. The two substrates with modifications, the frosted sand-blasted substrates and the polysine coated substrates show a decrease in adhesion energy over time. The un-modified plain borosilicate glass slide shows minimal changes in adhesion energy over time. For the

frosted substrates N = 72, for the plain substrates N = 66 and for the polysine coated substrates N = 59. The initial time point of 300 seconds (5 minutes) in figure 4.16 was chosen because at this time a significant enough amount of crack propagation has taken place and measurements of radial stretch are more accurate. The end point of 2000 seconds in figure 4.16 was chosen because this it the least amount of time it took any of the samples to completely delaminate, and all data displayed was based on this time.

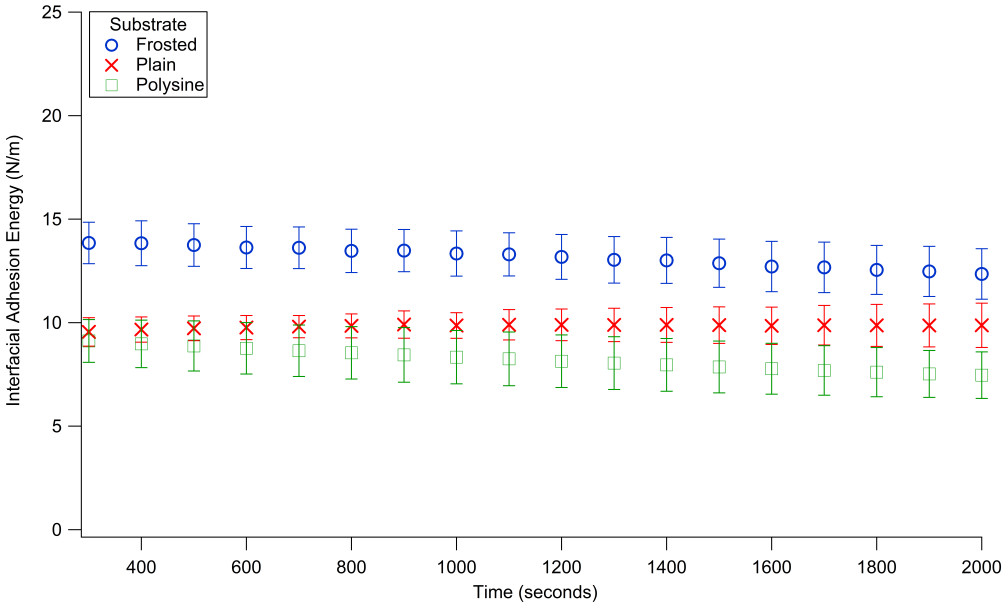

FIGURE 4.16: The interfacial adhesion energy plotted as a function of time. The two substrates with modifications show a decrease in energy over time while the un-modified plain substrate shows a constant interfacial energy over time. Each plot is the average of the tests conducted on the $300\mu m$, $350\mu m$ and $400\mu m$ radius samples.

Average Adhesion Energy (J/m^2)		
Frosted	Plain	Polysine
13±0.45	9.8±0.08	8.2±0.47

TABLE 4.3: The average values of the adhesion energy between 300 seconds and 2000 seconds.

4.5 Discussion

The polysine coated borosilicate glass substrates had the lowest interfacial adhesion energy of the three substrates tested. Polysine is a coating applied to glass slides to promote cell adhesion, but is not designed to promote adhesion to the polymer tested. Ultimately the experimental results showed an overall reduction in interfacial adhesion energy. There is also a slight decrease in the adhesion energy as crack propagation progresses, as was observed with the frosted glass slides.

Experiments have been conducted on HEMA-DMAEMA stimuli-responsive hydrogels to determine interfacial adhesion energy between the hydrogel and different substrates. HEMA-DMAEMA is a cross-linked co-polymer that can swell in acidic external buffer solutions. For those substrate modifications investigated, the interfacial energy over the course of crack propagation decreased. For the un-modified substrates this did not occur and remained a constant throughout the swelling process.

Surface morphology, chemical conditions and the application of surface forces all play a role in how adhesion occurs. The physics of adhesion can be groups into two categories, mechanical and chemical adhesion. Mechanical adhesion can be roughly segmented into macro and micro mechanical analogs. Mechanical adhesion occurs when one material, in a liquid form, seeps into the cracks and irregularities of a surface. When that material solidifies it becomes locked into the surface creating this mechanical type of attachment. Chemical adhesion is characterized by chemical bonds that occur at the surface of a material. Often times the difference in surface energies as well as the chemical bonding

that takes place locks the two surfaces together. This type of chemical bonding can become very strong.

Three substrates were tested, all borosilicate glass slides, two with different surface modifications. For the substrates that were sand-blasted to give a frosted appearance the interfacial surface energy was highest. It is hypothesized that the pre-polymer solution interlocks with the topology of the surface of the substrate and when polymerization occurs. This creates a situation on the interface in which both mechanical and chemical adhesion has occurred. The osmotic pressure caused by the diffusion of ionic species into the gel as well as the additional formation of H_2O that occurs supplies enough energy for this chemical and mechanical adhesion to be overcome and the gel to detach from the surface of the substrate and an interfacial crack to propagate. For the frosted substrate there are more sites for mechanical adhesion to occur, promoting higher interfacial adhesion.

In the experimental set-up used in this paper the axial constraint of the hydrogel prevents mode I loading and the delamination process occurs only in mode II. The strain energy formulation used to analyze these experiments deals only with the hydrogel and considers the substrate to be a rigid surface that only contributes to the boundary conditions of the problem. The strain energy release rate would normally have two terms. In our experimental setup the hydrogel itself is supplying the driving force for crack propagation and we can ignore the work done by external forces. This driving force is internal to the system which separates this adhesion method from others previously used. In many tests, such as the peel or pull test, the blister or beam bending tests, the driving force for

delamination is externally supplied. In this test method the driving force for delamination is supplied by the material itself. This allows one to test these materials *in-situ* thus we can mimic conditions that would actually be encountered during the normal use of a microfluidic device.

4.6 Conclusion

This experimental method illustrated the characterization of the interfacial energy between HEMA-DMAEMA stimuli-responsive hydrogels and the borosilicate glass slides tested with different surface modifications. This is a generalizable method capable of characterizing the relative adhesion strength of the different hydrogel/substrate interfaces. It was determined that the process of polymerization results in variable adhesion at the interface depending on substrate surface conditions. This knowledge expands our ability to quantify adhesion at such interfaces and allows microfluidic device designers to use this information strategically in microfluidic devices.

4.7 Acknowledgements

I would like to acknowledge helpful conversations that I have had with Dr. Mehrdad Arjmand, Suehelay Acevado-Acevado. Additionally I would like to thank Dr. David Beebe for use of his lab during the fabrication of the hydrogel samples.

Bibliography

[1] A.K.Agarwal, L.Dong, D.J.Beebe, and H.Jiang. Autonomously-triggered microfluidic cooling using thermo-responsive hydrogels. *Lab on a Chip*, 7(3):310–315, 2007.

[2] A.K.Henning. Microfluidics mems. In *Aerospace Conference, IEEE Proceedings*, volume 1(21), pages 471–486, 1998.

[3] Alireza Ousati Ashtiani and Hongrui Jiang. Thermally actuated tunable liquid microlens with sub-second response time. *Applied Physics Letters*, 103(11):111101, 2013.

[4] Erik Asmussen and Anne Peutzfeldt. Surface energy characteristics of adhesive monomers. *Dental Materials*, 14(1):21–28, 1998.

[5] D.J. Beebe, J.S. Moore, J.M. Bauer, Q. Yu, R.H. Liu, C. Devadoss, and B.H. Jo. Functional hydrogel structures for autonomous flow control inside microfluidic channels. *Nature*, 404(6778)(588-590), 2000.

[6] CC Benjamin, JC Springmann, SA Chindhy, and WC Crone. Experimental tools for responsive hydrogel characterization. In Society of Experimental Mechanics, editor, *Fracture and Fatigue, Volume 7: Conference Proceeding Society of Experimental Mechanics*, pages 7–11. Springer, 2014.

[7] Jason A Burdick, Ali Khademhosseini, and Robert Langer. Fabrication of gradient hydrogels using a microfluidics/photopolymerization process. *Langmuir*, 20(13): 5153–5156, 2004.

[8] Chaenyung Cha, Eleni Antoniadou, Minkyung Lee, Jae Hyun Jeong, Wylie W Ahmed, Taher A Saif, Stephen A Boppart, and Hyunjoon Kong. Tailoring hydrogel adhesion to polydimethylsiloxane substrates using polysaccharide glue. *Angewandte Chemie International Edition*, 52(27):6949–6952, 2013.

[9] Yeou-Shin Chang, Yeh-Hung Lai, and David A Dillard. The constrained blister—a nearly constant strain energy release rate test for adhesives. *The Journal of Adhesion*, 27(4):197–211, 1989.

[10] WT Chen and TF Flavin. Mechanics of film adhesion: Elastic and elastic-plastic behavior. *IBM Journal of Research and Development*, 16(3):203–213, 1972.

[11] L. Dong and H. Jiang. ph-adaptive microlenses using pinned liquid-liquid interfaces actuated by ph-responsive hydrogel. *Applied Physics Letters*, 81(21):211120, 2006.

[12] D.T.Eddington and D.J.Beebe. A valved responsive hydrogel microdispensing device with integrated pressure source. *Journal of Microelectromechanical Systems*, 13:586–593, 2004.

[13] D.T.Eddington and D.J.Beebe. Development of a disposable infusion system for the delivery of protein therapeutics. *Biomedical Microdevices*, 7(3):223–230, 2005.

[14] D.T.Eddington, R.H. Liu, J.S.Moore, and D.J.Beebe. An organic self-regulating microfluidic system. *Lab Chip*, 1:96–99, 2001.

[15] M. Elwenspoek, T.S.J. Lammerink, R. Miyakei, and J.H.J. Ruitman. Towards integrated microliquid handling systems. *J. Micromechanics and Microengineering*, 4: 227–245, 1994.

[16] BA Firestone and RA Siegel. Kinetics and mechanisms of water sorption in hydrophobic, ionizable copolymer gels. *Journal of applied polymer science*, 43(5):901–914, 1991.

[17] Alan D Freed and Beth Jorgensen. *Soft solids: A primer to the theoretical mechanics of materials*. Create Space Independent Publishing Platform, 2012.

[18] F.U.Gast, P.S.Dittrich, P.Schwille, M.Weigel, M.Mertig, J.Opitz, U.Queitsch, S.Diez, B.Lincoln, F.Wottawah, S.Schinkinger, J.Guck, J.Kas, J.Smolinski, K.Salchert, C.Werner, C.Duschl, M.S.Jager, K.Uhlig, P.Geggier, and S.Howitz. The microscopy cell (miccell), a versatile modular flowthrough system for cell biology, biomaterial research, and nanotechnology. *Microfluidics and Nanofluidics*, 2(1):21–36, 2006.

[19] P. Gravesen, J. Branebjerg, and O.S. Jensen. Microfluidics - a review. *J. Micromechanics*, 3:168–182, 1993.

[20] Alan A Griffith. The phenomena of rupture and flow in solids. *Philosophical transactions of the royal society of london. Series A, containing papers of a mathematical or physical character*, pages 163–198, 1921.

[21] Adam Hatch, Georg Hansmann, and Shashi K Murthy. Engineered alginate hydrogels for effective microfluidic capture and release of endothelial progenitor cells from whole blood. *Langmuir*, 27(7):4257–4264, 2011.

[22] Roland Jacobsson. Measurement of the adhesion of thin films. *Thin Solid Films*, 34 (2):191–199, 1976.

[23] J.Kim, B.Kim, J.Ryu, Y.Jeong, J.Park, H.C.Kim, and K.Chun. Potential of thermosensitive hydrogel as an actuator. *Japanese Journal of Applied Physics, Part 1: Regular Papers and Short Notes and Review Papers*, 44:5764–5768, 2005.

[24] B.D. Johnson, J.M. Bauer, D.J. Niedermaier, W.C. Crone, and D.J. Beebe. Experimental techniques for mechanical characterization of hydrogels at the microscale. *Experimental Mechanics*, 44(1):21–28, 2004.

[25] J.Y.Park, H.J.Oh, D.J.Kim, J.Y.Baek, and S.H.Lee. A polymeric microfluidic valve employing a ph-responsive hydrogel microsphere as an actuating source. *J. Micromechanics and Microengineering*, 16(3):656–663, 2006.

[26] J Kim, KS Kim, and YH Kim. Mechanical effects in peel adhesion test. *Journal of adhesion science and technology*, 3(1):175–187, 1989.

[27] Jim H Kou, Gordon L Amidon, and Ping I Lee. ph-dependent swelling and solute diffusion characteristics of poly (hydroxyethyl methacrylate–co–methacrylie acid) hydrogels. *Pharmaceutical research*, 5(9):592–597, 1988.

[28] T Krupenkin, Shu Yang, and P Mach. Tunable liquid microlens. *Applied Physics Letters*, 82(3):316–318, 2003.

[29] W.O. Kwang and H.A. Chong. A review of microvalves. *J. Micromechanics*, 16 (R13), 2006.

[30] Yeh-Hung Lai and David A Dillard. An elementary plate theory prediction for strain energy release rate of the constrained blister test. *The Journal of Adhesion*, 31(2-4): 177–189, 1990.

[31] M.E.Harmon, M.Tang, and C.W.Frank. A microfluidic actuator based on thermoresponsive hydrogels. *Polymer*, 44(16):4547–4556, 2003.

[32] J. Moorthy, G.A. Mensing, D. Kim, S. Mohanty, D.T. Eddington, W.H. Tepp, E.A. Johnson, and D.J. Beebe. Microfluidic tectonics platform: A colorimetric, disposable botulinum toxin enzyme-linked immunosorbent assay system. *Electrophoresis*, (10-11):1705–1713, 2004.

[33] MJ NAPOLITANO, A CHUDNOVSKY, and A MOET. The constrained blister test-a new approach to interfacial adhesion measurements. In *ABSTRACTS OF PAPERS OF THE AMERICAN CHEMICAL SOCIETY*, volume 194, pages 158–PMSE. AMER CHEMICAL SOC 1155 16TH ST, NW, WASHINGTON, DC 20036, 1987.

[34] MJ Napolitano, A Chudnovsky, and A Moet. The constrained blister test for the energy of interfacial adhesion. *Journal of Adhesion Science and Technology*, 2(1): 311–323, 1988.

[35] JE Pawel and CJ McHargue. Analysis of pull tests for determining the effects of ion implantation on the adhesion of iron films to sapphire substrates. *Journal of adhesion science and technology*, 7(8):845–852, 1993.

[36] Yong Qiu and Kinam Park. Environment-sensitive hydrogels for drug delivery. *Advanced drug delivery reviews*, 64:49–60, 2012.

[37] KR Rajagopal and AR Srinivasa. On the response of non-dissipative solids. In *Proceedings of the Royal Society of London A: Mathematical, Physical and Engineering Sciences*, volume 463, pages 357–367. The Royal Society, 2007.

[38] Kumbakonam R Rajagopal. On implicit constitutive theories. *Applications of Mathematics*, 48(4):279–319, 2003.

[39] Maria Rillosi and Graham Buckton. Modelling mucoadhesion by use of surface energy terms obtained from the lewis acid–lewis base approach. ii. studies on anionic, cationic, and unionisable polymers. *Pharmaceutical research*, 12(5):669–675, 1995.

[40] Eric K Sackmann, Anna L Fulton, and David J Beebe. The present and future role of microfluidics in biomedical research. *Nature*, 507(7491):181, 2014.

[41] Edward B Saubestre, Lawrence J Durney, Juan Hajdu, and Edwin Bastenbeck. The adhesion of electrodeposits to plastics. *Plating*, 52(10):982–1000, 1965.

[42] S. Shoji and M. Esashi. Microflow devices and systems. *J. Micromechanics*, 4: 157–171, 1994.

[43] AJM Spencer. Constitutive theory for strongly anisotropic solids. In *Continuum theory of the mechanics of fibre-reinforced composites*, pages 1–32. Springer, 1984.

[44] M Stamm. *Polymer Surfaces and Interfaces*. Springer, 2008.

[45] Leslie Ronald George Treloar. *The physics of rubber elasticity*. Oxford University Press, USA, 1975.

[46] Karel Vlassak, L van Holm, Luc Duchateau, Jozef Vanderleyden, and R de Mot. Isolation and characterization of fluorescent pseudomonas associated with the roots of rice and banana grown in sri lanka. *Plant and Soil*, 145(1):51–63, 1992.

[47] Yueguang Wei and John W Hutchinson. Interface strength, work of adhesion and plasticity in the peel test. In *Recent Advances in Fracture Mechanics*, pages 315–333. Springer, 1998.

[48] George M Whitesides. The origins and the future of microfluidics. *Nature*, 442(7101): 368–373, 2006.

[49] Yong Xiang, Xi Chen, and Joost J Vlassak. The mechanical properties of electroplated cu thin films measured by means of the bulge test technique. In *MRS Proceedings*, volume 695, pages L4–9. Cambridge Univ Press, 2001.

[50] Qing Yu, Joseph M Bauer, Jeffrey S Moore, and David J Beebe. Responsive biomimetic hydrogel valve for microfluidics. *Applied Physics Letters*, 78(17):2589–2591, 2001.

[51] Xuefeng Zeng and Hongrui Jiang. Tunable liquid microlens actuated by infrared light-responsive hydrogel. *Applied Physics Letters*, 93(15):151101, 2008.

Chapter 5

Future Direction

5.1 Future Directions

(2 - hydroxyethyl methacrylate) (HEMA) 2 - (dimethylamino) ethyl methacrylate (DMAEMA) stimuli responsive hydrogels are fascinating materials that have great potential as sensors and actuators in microfluidic devices. They represent a new classification of materials that is very new to the mechanics literature, that being an implicit elastic solid. Much of the study of stimuli-responsive hydrogels has come under the assumption that these polymers, although viscoelastic in nature, at their core obey a emplicit elastic constitutive law. The coupled, multi-physics field equations that have been developed along these lines have had some measure of success in describing the mechanics of these hydrogels. One issue arises when a researcher studying the large body of literature associated with these responsive hydrogels discovers that there is not one single consensus on what the

correct set of field equations should be. It is my believe that a different approach should be taken. When HEMA-DMAEMA swells from diffusion of ionic species into the hydrogel osmotic and hydrostatic pressure govern the stress field. Since diffusion is governed by geometry, the stress field generated by diffusion is governed by geometry. The stresses in this material are path dependence, or another way of putting this, the current state of stress is implied by the prior state of stress. It is the authors belief that use of implicit elastic theories is the future direction of the mechanical description of HEMA-DMAEMA.

Appendix A

Continuum Mechanics Review:

A.1 Kinematics

When we describe the motion of a particle by definition the particle has mass but no volume. Thus the description of the motion is strictly translational. When the volume of a body needs to be taken into account but the body can be assumed to be 'rigid' the body is now a collection of particles. We now have to describe not only the translational motion but the rotational motion of the body. We do not, however, need to account for the motion of the particles relative to one another because of the rigid body assumption. This all changes when a body can be deformed. Now the position of all particles relative to one another can change. Now not only does the translational and rotational motion have to be taken into account the motion of the particles relative to one another needs to be address. The discipline of continuum mechanics addresses this particular problem.

Take a body $\mathcal{B}$ with a volume consisting of particles $\mathcal{P}$ that occupies a region of space Ω at time t. We describe the motion of of the particles $\mathcal{P}$ in two general ways. Those being the reference (*Lagrangian*) description and the spatial (*Eulerian*) description.

In the Lagrangian description the configuration of the body in question is taken to be the initial configuration. This is most commonly the unstressed configuration but this restriction is not necessary, at time $t = 0$. In the reference configuration we fix all the particles in place and denote their positions, relative to an external reference point, with the vector $\mathrm{X}_I = [X_1, X_2, X_3]$. From this point we follow the path of each particle as it propagates forward in time. At some time t we denote the current position of a particle, with reference to the same external origin, by the vector $\mathrm{x}_i = [x_1, x_2, x_3]$. The vector $\mathbf{x}$ refers to the particle in the current or *spatial* configuration. We can write the current position x_i as a function of the reference position X_I and any time dependent displacement $\mathbf{u}$ that occurs that changes the reference position into the final position. Note that any lower case subscripts refer to the current configuration and any upper case subscripts refer to the reference configuration.

$$\mathrm{x}_i = \mathrm{X}_I + \mathrm{u}_i. \tag{A.1}$$

In general we can write the current position $\mathbf{x}$ as a function of the initial position and time,

$$\mathbf{x} = \mathcal{X}(\mathbf{X}, t) \tag{A.2}$$

If we take a differential of the current position,

$$\mathrm{dx}_i = \frac{\partial \mathcal{X}_i}{\partial \mathrm{X}_J}\mathrm{dX}_J + \frac{\partial \mathcal{X}_i}{\partial t}dt, \tag{A.3}$$

We define the *deformation gradient* as,

$$\mathrm{F}_{iJ} = \frac{\partial \mathcal{X}_i}{\partial \mathrm{X}_J} = \lambda_{iJ}, \tag{A.4}$$

and this represents the spatial mapping between the reference and current configurations. The symbol λ is the component representation of the deformation gradient. Using equation (A.1) in equation (A.4) we find,

$$\mathrm{F}_{iJ} = \frac{\partial(\mathrm{X}_I + \mathrm{u}_i)}{\partial \mathrm{X}_J} = \delta_{iJ} + \frac{\partial \mathrm{u}_i}{\partial \mathrm{X}_J}, \tag{A.5}$$

where the term $\frac{\partial \mathrm{u}_i}{\partial \mathrm{X}_J}$ is the *displacement gradient*. From this we note that this partial derivative is taken with time being constant, therefore we can define the relationship,

$$\mathrm{dx} = \mathrm{F} \cdot \mathrm{dX}. \tag{A.6}$$

We define the finite strain tensor as,

$$E_{iJ} = \frac{1}{2}(C_{iJ} - \delta_{iJ}), \tag{A.7}$$

where C_{iJ} is the right Cauchy-Green deformation tensor, $C_{iJ} = F_{ki}F_{kJ}$.

A.2 General Theorems:

There are two divisions in mechanics, those being vector mechanics and analytical mechanics. Vector mechanics isolates an object from its surrounding and designates all the forces acting on the object through a free-body diagram. In this field of mechanics many problems become almost intractable when the geometry being studied is not optimal. For many situations the geometry is so complicated that writing down field equations can become next to impossible to do.

The realm of analytical mechanics makes it possible to write down field equations regardless of geometrical constraints through potential functions. This enables the derivation of field equations with relative ease provide one have a defined form for the potential functions in question. Analytical mechanics revolves around Hamilton's principle. Briefly stated Hamilton's principle is,

Among the admissible motions a system can take, the actual motion of the system is such that the following integral expression,

$$I = \int_{t_1}^{t_2} (T - U) + W + C \text{ dt}$$

is stationary with respect to time.

This can be written compactly as,

$$\int_{t_1}^{t_2} [\delta(T - U) + \delta W + \delta C] \text{ dt}, \tag{A.8}$$

where T is the kinetic energy, U is the potential energy, W is the virtual work done and C are the constraints on the system. We will now derive the field equations for an elastic solid under the assumptions of no constraint forces. We however do not limit ourselves to conservative systems, both conservative and non-conservative systems obey Hamilton's principle.

The kinetic energy is defined as,

$$T = \int_B \frac{1}{2} \rho \mathbf{v} \cdot \mathbf{v} dV, \tag{A.9}$$

where ρ is density and $\mathbf{v}$ is velocity. The integral is taken over the entire body B of volume V. The potential energy is always taken to be a function of the deformation gradient $\mathbf{F}$. Therefore the potential energy can be written as,

$$U = \int_B \rho\psi(\mathbf{F})dV, \tag{A.10}$$

where $\psi(\mathbf{F})$ is the strain energy density function which is function of the deformation gradient. The virtual work performed on an elastic solid is given as,

$$W = \int_{V_B} \rho\mathbf{b}dV + \int_{S_B} \mathbf{t} \cdot dS, \tag{A.11}$$

where b is the body force and t is the surface traction vector. In order to find the variation in these quantities we re-write the kinematic variables in terms of a small variation in that variable.

$$\begin{aligned} \mathbf{u}^* &= \mathbf{u} + \alpha\delta u, \\ \mathbf{v}^* &= \mathbf{v} + \alpha\delta\dot{u}, \\ \mathbf{F}^* &= \mathbf{I} + \frac{\partial \mathbf{u}}{\partial X} + \alpha\frac{\partial \delta u}{\partial X}. \end{aligned} \tag{A.12}$$

These variations are written in terms of the small variation δu and the only requirement on this variation is that is vanishes at the limits of the interval t_1 to t_2. To minimiz the kinetic and potential energy as well at the virtual work we write these functions in terms of their variations then minimize the functions with respect to the parameter α. In what

follows I will give the final expressions for the variations in kinetic and potential energy as well as the variations in virtual work.

$$\begin{aligned} \delta T &= -\int_{V_B} \rho \mathbf{a} \cdot \delta u dV, \\ \delta U &= \int_{S_B} \sigma \mathbf{n} \cdot \delta u dS - \int_{V_B} \nabla \cdot \sigma \cdot \delta u dV, \\ \delta W &= \int_{V_B} \rho \mathbf{b} \cdot \delta u dV + \int_{S_B} \mathbf{t} \cdot \delta u dS, \end{aligned} \tag{A.13}$$

where σ is the *Cauchy* stress tensor. Using equation (A.13) in Hamilton's principle (A.8) and grouping like terms we arrive at,

$$\int_{t_1}^{t_2} \left[\int_{V_B} (\rho \mathbf{b} + \nabla \cdot \sigma - \rho \mathbf{a}) \cdot \delta u dV + \int_{S_B} (\mathbf{t} - \sigma \mathbf{n}) \cdot \delta u dS \right] dt = 0 \tag{A.14}$$

For this equation to be valid for an arbitrary variation δu each integral has to vanish. This leaves us with the familiar principle of linear momentum,

$$\nabla \cdot \sigma + \rho \mathbf{b} = \rho \mathbf{a}$$

and the familiar boundary condition,

$$\mathbf{t} = \sigma \mathbf{n}$$

Continuum Mechanics General Theorems	
Linear Momentum Conservation	$\frac{\partial \sigma_{ij}}{\partial x_j} + b_i = \rho \frac{Dv_i}{Dt}$
Angular Momentum Conservation	$\sigma_{ij} = \sigma_{ji}$
Mass Conservation	$\frac{D\rho}{Dt} + \rho \frac{\partial v_i}{\partial x_i} = 0,\ J = det(\mathbf{F})$
Compatibility	$F_{ij} = \delta_{ij} + \frac{\partial u_i}{\partial X_j}$
Strain Tensor	$E_{ij} = \frac{1}{2}(F_{ki}F_{kj} - \delta_{ij})$
Constitutive Equation	$s_{ij} = \frac{\partial \psi(F_{ij})}{\partial F_{ij}},\ \sigma_{ij} = J^{-1} s_{ik} F_{jk}$
Material Derivative	$\frac{Df_i}{Dt} = \frac{\partial f_i}{\partial t} + v_k \frac{\partial f_i}{\partial x_k}$

TABLE A.1: General theorems of continuum mechanics

which is commonly known as the *Cauchy traction relation.*

A similar procedure can be used to derive the conservation of mass and the conservation of angular momentum. Summarized in table A.1 are the main theorems of continuum mechanics. These theorems along with a definition for a constitutive relationship between stresses and strains allows one to analyze the motion of a continuum body. All continuum bodies obey the fundamental theorem of continuum mechanics. What separates each theory from one another is how the specific theory defines the stress/strain relationship (constitutive equations) and the strain/displacement relationship (compatibility). Once defined these theorems are applied to the fundamental theorems of continuum mechanics. We will now briefly review the theories of linear elasticity, linear viscoelasticity and the non-linear theories of rubber elasticity and morphoelasticity.

A.3 Finite Elasticity

The elasticity of materials undergoing large deformations has been a subject of study for much of the past century. The elastic response of rubber like materials was grounded in a

solid foundation based on the theories of finite elasticity and this has given birth to solid mechanics being applied to many different disciplines. Fields of study such as thermo and electromechanics, mixture theory, wave propagation, soil mechanics as well as many others are a result of finite elasticity theory. The success of finite elasticity in these fields cannot be understated. This success has lead to the application of solid mechanics in biological materials, mulitpolar (cosserat) materials, constrained materials as a brief list. Solid mechanics is studies by professionals in fields such as applied mechanics, engineering, chemistry and physics.

Finite elasticity can be roughly grouped into two separate fields. Those being *Explicit elasticity* and *Implicit Elasticity* where the distinction in the two fields is due to the constitutive relationships. In a lot of explicit elasticity theories engineering constants such as Young's, shear modulus and the poisson ratio are constants. For the Young's modulus it can be shown from the one dimensional version of Hooke's law,

$$\frac{\sigma}{\varepsilon} = E. \tag{A.15}$$

where the Young's modulus has units of stress and is a constant. In finite elasticity stress is often represented as a function of stretch and not strain. It is often found that the stress/stretch relationship cannot is often nonlinear. The **Tangent Modulus** is defined as the derivative of the stress and the stretch,

$$\frac{\partial T(\lambda)}{\partial \lambda} = E(\lambda) \tag{A.16}$$

where the tangent modulus is no longer a constant and now can depend on the stretch. The relationship between strain and stretch is another subject for much debate. The main idea that makes continuum mechanics so applicable to so many different fields is the concept of mapping physics points in space from one configuration to another. This idea is central to the fields of solid and fluid mechanics were many theories depend heavily on the observers point of view.

Stretch and strain are defined as unitless quantities but they inherently mappings between reference and current configurations. While strain is an engineering quantity that is well understood and used extensively in mechanics of materials and linear elasticity stretch is a quantity that is specifically defined as the components of the deformation gradient and this becomes the preferred measure of displacement because it takes into account the differences of the separate configurations.

Hencky strain which is sometimes referred to as 'natural strain' or 'logarithmic strain' is a one dimensional measure of strain that relates to stretch as,

$$\varepsilon = ln(\lambda). \tag{A.17}$$

Engineering strain, which is most useful for small deformations, has the strain/stretch relationship given by,

$$\varepsilon = \lambda - 1. \tag{A.18}$$

While there is a whole field of study devoted to the many different measures of strain these two strain/stretch relationships are among the most commonly used.

Appendix B

Linear Elasticity

B.1 Small Strain Assumption

The theory of linear elasticity is a special branch of continuum mechanics that analyzes stress, recoverable displacements and recoverable strains in a solid body that is assumed to behave elastically. Using the assumption of small deformations allows us to consider the displacement gradient to be very small $\mathbf{u}\nabla \ll 1$. From this main assumption a few simplifications can be made.

Since displacements are extremely small the difference between the reference and spacial configurations are negligible and $x \simeq X$. The determinant of the deformation gradient, which is the ration of the final and initial volumes of the elastic body, are taken to be unity. Since deformations are small a taylor expansion can be performed on the strain energy density function. This leads to the linear elastic stress/strain relationship,

$$\sigma_{ij} = \sigma^r_{ij} + C_{ijkl}\varepsilon_{kl}, \tag{B.1}$$

where σ^r_{ij} is the residual stress and C_{ijkl} is a fourth order modulus tensor that relates stresses to strains. The main assumption that the displacement gradient is much less than unity allows us to write the compatibility condition for the strain tensor as,

$$\varepsilon_{ij} = \frac{1}{2}(u_{i,j} + u_{j,i}). \tag{B.2}$$

When the solid body is taken to be *elastically isotropic* the most general form of the fourth-order elastic modulus tensor, which is symmetric in ij or kl takes on the following form,

$$C_{ijkl} = \lambda\delta_{ij}\delta_{kl} + \mu[\delta_{ik}\delta_{jl} + \delta_{il}\delta_{jk}]. \tag{B.3}$$

when equation (B.3) is substituted into equation (B.1) the following constitutive equation is obtained,

$$\boxed{\sigma_{ij} = \lambda\delta_{ij}\varepsilon_{kk} + 2\mu\varepsilon_{ij},} \tag{B.4}$$

where μ and λ are Lamé constants. From Hooke's law we can solve for stresses in terms

of strains and get the relationship between the Lamé constants and the engineering constants,

$$\begin{aligned}
\varepsilon_{ij} &= \frac{1+\nu}{E}\sigma_{ij} - \frac{\nu}{E}\delta_{ij}\sigma_{kk}, \\
\varepsilon_{kk} &= \frac{1-2\nu}{E}\sigma_{kk}, \\
\sigma_{kk} &= \frac{E}{1-2\nu}\varepsilon_{kk}, \\
\varepsilon_{ij} &= \frac{1+\nu}{E}\sigma_{ij} - \frac{\nu}{E}\frac{E}{1-2\nu}\delta_{ij}\varepsilon_{kk}, \\
\sigma_{ij} &= \frac{E}{1+\nu}\varepsilon_{ij} + \frac{E\nu}{(1+\nu)(1-2\nu)}\delta_{ij}\varepsilon_{kk}.
\end{aligned} \tag{B.5}$$

From this we can make a one to one comparison and see the relationship between the Lamé constants and the engineering constants,

$$\lambda = \frac{E\nu}{(1+\nu)(1-2\nu)} \qquad \mu = G. \tag{B.6}$$

In total there are fifteen unknowns, six stress components, six strain components and three displacement components, and fifteen equations,

$$\text{Equilibrium (3)} \qquad \frac{\partial \sigma_{ij}}{\partial x_j} + \rho b_i = \rho \ddot{u}_i, \tag{B.7a}$$

$$\text{Compatibility (6)} \qquad \varepsilon_{ij} = \frac{1}{2}(u_{i,j} + u_{j,i}), \tag{B.7b}$$

$$\text{Hooke's Law (6)} \qquad \sigma_{ij} = C_{ijkl}\varepsilon_{kl}, \tag{B.7c}$$

These field equations must be satisfied on all interior points in a solid body. One the surface of the solid body either the three components of the Cauchy relationship,

$$t_i = \sigma_{ij} n_j, \tag{B.8}$$

or the three components of the surface displacement vector,

$$u_i^{inside} = u_i^{outside} \tag{B.9}$$

must be satified, or some combination of the two. The theory of linear viscoelasticity uses, as its basis, linear elasticity.

Appendix C

Linear Viscoelasticity:

When a load is suddenly applied to an elastic solid the material will respond with an instantaneous deformation that remains in this state until the load is removed. For a Newtonian viscous fluid the material will flow in response to the suddenly applied load. A viscoelastic material will respond to that load with an elastic deformation followed by a steady flow process. This phenomena is known as creep, or an increase in strain when the stress is held constant. Over time a viscoelastic material displays the phenomena known as relaxation or a gradual decrease in stress, when a suddenly applied strain is held constant. These two phenomena may be used as experimental methods to characterize materials. They are also relevant to the design and application of these materials

When strains are small, most solid bodies can be described using Hooke's law constitutive equation. In one dimension this gives a linear relationship between stress and strain that is governed by a modulus of elasticity,

$$\sigma = E\varepsilon, \tag{C.1}$$

where E is the Young's modulus of the solid body. On the other side of the spectrum a viscous fluid that is subject to a shear stress has the following constitutive relationship,

$$\sigma = \eta \frac{d\varepsilon}{dt}, \tag{C.2}$$

where η is the viscosity of the fluid and the stress depends not on the strain but the strain rate. All real materials, to some degree, are not exactly described as solid or fluid. Most materials exhibit viscous and elastic characteristics. A viscoelastic material is described by having its stress and strain relationship depend on time.

Viscoelastic behavior becomes apparent when the material displays creep, or an increase in strain when the stress is held constant. The *creep compliance* is given as,

$$J(t) = \frac{\varepsilon(t)}{\sigma_o}, \tag{C.3}$$

where σ_o is the instantaneously applied stress and $J(t)$ is the creep compliance. When the material displays relaxation or a gradual decrease in stress for a given strain that is held constant. The *relaxation modulus* is given as,

$$E(t) = \frac{\sigma(t)}{\varepsilon_o}, \tag{C.4}$$

where ε_o is the instantaneously applied strain and $E(t)$ is the relaxation modulus.

C.1 Boltzmann Superposition Integral

For the one-dimensional case, if we take a small increment of strain at time $t = 0$, the stress at time $t = \tau$ for a viscoelastic material can be determined by,

$$d\sigma(\tau) = E(\tau)d\varepsilon(0), \tag{C.5}$$

where $E(\tau)$ is the time dependent relaxation modulus. If after this first time increment the material is subjected to another, but different, incremental strain from time $t = \tau$ to a later time t the stress response will be different and can be shown to be,

$$d\sigma(t) = E(t - \tau)d\varepsilon(\tau). \tag{C.6}$$

To find the total stress one needs only to integrate over the entire time history,

$$\sigma(t) = \int_0^t E(t - \tau)d\varepsilon(\tau), \tag{C.7}$$

which is known as a *Stieltjes* integral which allows $\varepsilon(\tau)$ to have instantaneous jumps in time. If $\varepsilon(t)$ is differentiable equation (C.7) can be written as,

$$\sigma(t) = \int_o^t E(t-\tau)\frac{d\varepsilon(\tau)}{d\tau}d\tau, \tag{C.8}$$

Equation (C.8) is known as the *Boltzmann superposition integral*. The Boltzmann superposition can be generalized to three dimensions as,

$$\boxed{\sigma_{ij}(t) = \int_0^t C_{ijkl}(t-\tau)\frac{d\varepsilon_{kl}(\tau)}{d\tau}d\tau,} \tag{C.9}$$

and

$$\boxed{\varepsilon_{ij}(t) = \int_0^t S_{ijkl}(t-\tau)\frac{d\sigma_{kl}(\tau)}{d\tau}d\tau.} \tag{C.10}$$

C.2 Deviatoric Stress/Strain

If one defines the *deviatoric* stress and strain as,

$$s_{ij} = \sigma_{ij} - \frac{1}{3}\delta_{ij}\sigma_{kk}, \tag{C.11a}$$

$$\epsilon_{ij} = \varepsilon_{ij} - \frac{1}{3}\delta_{ij}\varepsilon_{kk}, \tag{C.11b}$$

where the trace of the deviatoric stress and strain are both zero respectively and $\frac{1}{3}\sigma_{kk}$ and $\frac{1}{3}\varepsilon_{kk}$ are the hydrostatic pressure and dilitational strain. Using equation (C.11b) one can write the total strain in terms of its deviatoric and dilitational parts,

$$\varepsilon_{ij} = \epsilon_{ij} + \frac{1}{3}\delta_{ij}\varepsilon_{kk}. \tag{C.12}$$

Thus the stress-strain relationship becomes,

$$\sigma_{ij} = \frac{1}{3}(3\lambda + 2\mu)\delta_{ij}\varepsilon_{kk} + 2\mu\epsilon_{ij}, \tag{C.13}$$

and using the fact that $\epsilon_{kk} = 0$ the hydrostatic pressure becomes,

$$\sigma_{kk} = (3\lambda + 2\mu)\varepsilon_{kk}. \tag{C.14}$$

Using equations (C.13) and (C.14) in equation (C.11a) we arrive at the following relationship for the deviatoric stress and strain,

$$s_{ij} = \frac{1}{3}(3\lambda + 2\mu)\delta_{ij}\varepsilon_{kk} + 2\mu\epsilon_{ij} - \frac{1}{3}\delta_{ij}\sigma_{kk}, \tag{C.15}$$

$$= \frac{1}{3}(3\lambda + 2\mu)\delta_{ij}\varepsilon_{kk} + 2\mu\epsilon_{ij} - \frac{1}{3}(3\lambda + 2\mu)\delta_{ij}\varepsilon_{kk}, \tag{C.16}$$

$$= 2\mu\epsilon_{ij}, \tag{C.17}$$

and using the Boltzmann superposition principle we can write the deviatoric viscoelastic constitutive equation as,

$$\boxed{s_{ij}(t) = \int_0^t 2\mu(t-\tau)\frac{d\epsilon_{ij}(\tau)}{d\tau}d\tau.} \tag{C.18}$$

C.3 Dynamic Response

In one dimension if one applies a sinusoidally varying strain,

$$\varepsilon(t) = \varepsilon_o \exp[i\omega t], \tag{C.19}$$

where the angular frequency ω is related to the frequency f in Hz by $\omega = 2\pi f$. The stress response can be determined using the Boltzmann superposition integral (C.8),

$$\sigma(t) = i\omega\varepsilon_o \int_0^\infty E(t-t')\exp[i\omega t']dt'. \tag{C.20}$$

If we make a change in variables, $t - t' = \tau$ and $-dt' = d\tau$ we can re-write equation (C.20) as,

$$\sigma(t) = -i\omega\varepsilon_o \int_0^\infty E(\tau)\exp[i\omega(t-\tau)]d\tau, \tag{C.21}$$

$$= -i\omega\varepsilon_o \exp[i\omega t] \int_0^\infty E(\tau)\exp[-i\omega\tau]d\tau, \tag{C.22}$$

$$= \varepsilon(t)\left(\omega \int_0^\infty E(\tau)sin(\omega\tau)d\tau + i\omega \int_0^\infty E(\tau)cos(\omega\tau)d\tau\right), \tag{C.23}$$

$$= E^*(\omega)\varepsilon(t), \tag{C.24}$$

where we note that the term in parenthesis is a complex valued term defined as the *dynamic modulus*, $E^*(\omega) = E' + iE''$,

$$E'(\omega) = \omega \int_0^\infty E(\tau)sin(\omega\tau)d\tau, \tag{C.25a}$$

$$E''(\omega) = \omega \int_0^\infty E(\tau)cos(\omega\tau)d\tau. \tag{C.25b}$$

We define E' as the *storage modulus* and E'' as the *loss modulus*.

Equations of Linear Viscoelasticity

The equations of linear viscoelasticity can be summed up as follows,

$$\text{Equilibrium (3)} \qquad \frac{\partial \sigma_{ij}}{\partial x_j} + \rho b_i = \rho \ddot{u}_i, \tag{C.26a}$$

$$\text{Compatibility (6)} \qquad \varepsilon_{ij} = \frac{1}{2}(u_{i,j} + u_{j,i}), \tag{C.26b}$$

$$\text{Boltzmann Integral (6)} \qquad \sigma_{ij} = \int_0^t C_{ijkl}(t-\tau)\frac{d\varepsilon_{kl}(\tau)}{d\tau}d\tau, \tag{C.26c}$$

Appendix D

Stretch Data Collection:

D.1 Hydrogel Thresholding

```
% ------------------------------------------------------------------------
%
% The HydrogelThreshold code is used to take a stack of swelling hydrogel
% post images and analyze each post.  First the image is loaded into memory
% and the hydrogel posts are isolated from the rest of the image.  The
% cropped images are then thresholded so that measurements can be made of
% the swelling of the outer diameter
%
% Chandler Benjamin 2017
%
% ------------------------------------------------------------------------

clc          % Clears screen
clear        % Clears variables
format short % Makes formatting short for program

```

```
17 % Prompt for calibration file
18 % uigetfile prompts to search computer for a file.
19
20 % % % image(im_data);
21 prompt = {'Enter Radius'};
22 dlg_title           = 'Radius';
23 num_lines           = 1;
24 def                 = {'300'};
25 answer              = inputdlg(prompt,dlg_title,num_lines,def);
26 RefOuterRadius      = str2double(answer{1});
27
28 Pdate = PDate;          % Function call for date.
29
30 % Get image stack for analysis
31 % uigetfile prompts to search computer for a file.
32 [FileName,PathName] = uigetfile('*.tif','Select Image Stack');
33
34 %% Get image information
35 info = imfinfo([PathName FileName]);                % Loads image information
36 imagenumber     = numel(info);                      % Number of images
37 ImageOutside    = zeros(imagenumber,1);             % Outer diameter stack
38 ImageInside     = zeros(imagenumber,1);             % Inner diameter stack
39 ImageLoopNum    = zeros(imagenumber,1);             % Image Loop Number
40
41 % 1.  Reads first image.
42 % 2.  Crops image and gets the defined area of the croping.
43 A = imread([PathName FileName],1,'Info',info);
44 imshow(A);
45
46 % 1.  Displays current cropped image in the stack
47 % 2.  While loop records the following
48 %    i. Outter diameter of hydrogel
49 %   ii. Inner diameter(crack front)
50 %  iii. Always prompts to see if lines are correct
```

```
% 3.  Record image number in an array
% 4.  Read in next image in stack

prompt = {'Enter the number of posts'};
dlg_title = 'Post Number';
num_lines = 1;
def = {'6'};
answer = inputdlg(prompt,dlg_title,num_lines,def);
stack = str2double(answer{1});

pt1 = zeros(1,2);
pt2 = zeros(1,2);
pt3 = zeros(1,2);

s = 1;

for n = 1:stack
clc
Disp1   = ['This is stack ' num2str(n)];
disp(Disp1);

A = imread([PathName FileName],10,'Info',info);

% 1. Crops image and defines the cropping region.

[I1,rectang] = imcrop(A);
for k = 1:9:imagenumber

% 1. Load image.

A = imread([PathName FileName],k,'Info',info);
I = imcrop(A,rectang);

% 2. Turns image into a grayscale image
```

```
85
86  I = rgb2gray(I);
87
88  % 3. Normalization of the image.
89
90  [normim, mask, maskind] = ridgesegment(I, 12, 0.2);
91
92  % 5. Displays image.
93
94  imshow(normim);
95  DispX   = ['This is image number ' num2str(s)];
96  disp(DispX);
97
98  % Outer Radius
99  [XT1,YT1] = ginput(3);
100 pt1(1,1) = XT1(1,1);
101 pt1(1,2) = YT1(1,1);
102 pt2(1,1) = XT1(2,1);
103 pt2(1,2) = YT1(2,1);
104 pt3(1,1) = XT1(3,1);
105 pt3(1,2) = YT1(3,1);
106 [Cir1, Rad1] = calcCircle(pt1,pt2,pt3);
107
108 % Crack Length
109 [XT2,YT2,button] = ginput(1);
110 if button == 2
111 Rad2 = 0;
112 else
113 pt1(1,1) = XT2(1,1);
114 pt1(1,2) = YT2(1,1);
115 [XT2,YT2] = ginput(2);
116 pt2(1,1) = XT2(1,1);
117 pt2(1,2) = YT2(1,1);
118 pt3(1,1) = XT2(2,1);
```

```
119 pt3(1,2) = YT2(2,1);
120 [Cir2, Rad2] = calcCircle(pt1,pt2,pt3);
121 end
122
123 % Array for outer and crack lengths
124 RadiusCalc(s,1) = Rad1;
125 RadiusCalc(s,2) = Rad2;
126 s = s+1;
127 end
128
129 s = 1;
130
131 % Loads data into crack length and stretch arrays
132 [M N]   = size(RadiusCalc);
133 RefOut  = RadiusCalc(1,1);
134
135 % Initialize data arrays
136 CInt    = zeros(M,1);
137 Crack   = zeros(M,1);
138 Stretch = zeros(M,1);
139
140 for k = 1:M
141 Crack(k,1)      = RefOut - RadiusCalc(k,2);
142 Stretch(k,1)    = RadiusCalc(k,1)/RefOut;
143 CInt(k,1)       = Crack(k,1)/RefOut;
144 end
145
146 FinalCrack      = CInt.*RefOuterRadius;
147 FinalStretch    = Stretch.*RefOuterRadius;
148
149 % Open files to save data into
150 fid1 = fopen(['OuterDiameter' num2str(Pdate{1}) '_' num2str(n) '.txt'],'w');
151 fid2 = fopen(['CrackLength' num2str(Pdate{1}) '_' num2str(n) '.txt'],'w');
152 fid3 = fopen(['StretchStack' num2str(Pdate{1}) '_' num2str(n) '.txt'],'w');
```

```
153
154 % Get size data for stacks
155 [row1,col1] = size(FinalStretch(:,1));
156 [row2,col2] = size(FinalCrack(:,1));
157 [row3,col3] = size(Stretch(:,1));
158
159 % Formatting for fprintf function
160 z1 = repmat('%d\t',1,(col1-1));
161 z2 = repmat('%d\t',1,(col2-1));
162 z3 = repmat('%d\t',1,(col3-1));
163
164 % Writes data into file and saves
165 fprintf(fid1,[z1,'%d\n'],FinalStretch(:,1)');
166 fprintf(fid2,[z2,'%d\n'],FinalCrack(:,1)');
167 fprintf(fid3,[z3,'%d\n'],Stretch(:,1)');
168
169
170 end
171
172
173 %-------------------------------------------------------------------------
```

D.2 Date Acquisition

```
function [ Pdate ] = PDate( )
%------------------------------------------------------------------------
%
%   Function gets testing date
%
%------------------------------------------------------------------------

% Prompting for sample date
    prompt = {'What is the testing date? ex. (051511):'};
    dlg_title = 'Date on Test';
    num_lines = 1;
    def = {'011115'};
    Pdate = inputdlg(prompt,dlg_title,num_lines,def);

end
```

D.3 Measurement of Stretch and Crack Length

```
clc          % Clears screen
clear        % Clears variables
format short % Makes formatting short for program

% Prompt for calibration file
% uigetfile prompts to search computer for a file.

% % % image(im_data);
prompt = {'Enter Radius'};
dlg_title           = 'Radius';
num_lines           = 1;
def                 = {'300'};
answer              = inputdlg(prompt,dlg_title,num_lines,def);
RefOuterRadius      = str2double(answer{1});

Pdate = PDate;          % Function call for date.

% Get image stack for analysis
% uigetfile prompts to search computer for a file.
[FileName,PathName] = uigetfile('*.tif','Select Image Stack');

%% Get image information
info = imfinfo([PathName FileName]);                % Loads image information
imagenumber     = numel(info);                      % Number of images
ImageOutside    = zeros(imagenumber,1);             % Outer diameter stack
ImageInside     = zeros(imagenumber,1);             % Inner diameter stack
ImageLoopNum    = zeros(imagenumber,1);             % Image Loop Number

% 1.  Reads first image.
% 2.  Crops image and gets the defined area of the croping.
A = imread([PathName FileName],1,'Info',info);
imshow(A);
```

```
33
34 % 1.  Displays current cropped image in the stack
35 % 2.  While loop records the following
36 %    i. Outter diameter of hydrogel
37 %   ii. Inner diameter(crack front)
38 %  iii. Always prompts to see if lines are correct
39 % 3.  Record image number in an array
40 % 4.  Read in next image in stack
41
42 prompt = {'Enter the number of posts'};
43 dlg_title = 'Post Number';
44 num_lines = 1;
45 def = {'6'};
46 answer = inputdlg(prompt,dlg_title,num_lines,def);
47 stack = str2double(answer{1});
48
49 pt1 = zeros(1,2);
50 pt2 = zeros(1,2);
51 pt3 = zeros(1,2);
52
53 s = 1;
54
55 for n = 1:stack
56 clc
57 Disp1   = ['This is stack ' num2str(n)];
58 disp(Disp1);
59
60 A = imread([PathName FileName],10,'Info',info);
61 % 1. Crops image and defines the cropping region.
62 [I1,rectang] = imcrop(A);
63 for k = 1:9:imagenumber
64 % 1. Load image.
65 A = imread([PathName FileName],k,'Info',info);
66 I = imcrop(A,rectang);
```

```
67  % 2. Turns image into a grayscale image
68  I = rgb2gray(I);
69  % 3. Normalization of the image.
70  [normim, mask, maskind] = ridgesegment(I, 12, 0.2);
71  % 5. Displays image.
72  imshow(normim);
73  DispX   = ['This is image number ' num2str(s)];
74  disp(DispX);
75
76  % Outer Radius
77  [XT1,YT1] = ginput(3);
78  pt1(1,1) = XT1(1,1);
79  pt1(1,2) = YT1(1,1);
80  pt2(1,1) = XT1(2,1);
81  pt2(1,2) = YT1(2,1);
82  pt3(1,1) = XT1(3,1);
83  pt3(1,2) = YT1(3,1);
84  [Cir1, Rad1] = calcCircle(pt1,pt2,pt3);
85  % Crack Length
86  [XT2,YT2,button] = ginput(1);
87  if button == 2
88  Rad2 = 0;
89  else
90  pt1(1,1) = XT2(1,1);
91  pt1(1,2) = YT2(1,1);
92  [XT2,YT2] = ginput(2);
93  pt2(1,1) = XT2(1,1);
94  pt2(1,2) = YT2(1,1);
95  pt3(1,1) = XT2(2,1);
96  pt3(1,2) = YT2(2,1);
97  [Cir2, Rad2] = calcCircle(pt1,pt2,pt3);
98  end
99  % Array for outer and crack lengths
100 RadiusCalc(s,1) = Rad1;
```

```
101 RadiusCalc(s,2) = Rad2;
102 s = s+1;
103 end
104
105 s = 1;
106
107 % Loads data into crack length and stretch arrays
108 [M N]   = size(RadiusCalc);
109 RefOut  = RadiusCalc(1,1);
110 % Initialize data arrays
111 CInt    = zeros(M,1);
112 Crack   = zeros(M,1);
113 Stretch = zeros(M,1);
114
115 for k = 1:M
116 Crack(k,1)      = RefOut - RadiusCalc(k,2);
117 Stretch(k,1)    = RadiusCalc(k,1)/RefOut;
118 CInt(k,1)       = Crack(k,1)/RefOut;
119 end
120
121 FinalCrack      = CInt.*RefOuterRadius;
122 FinalStretch    = Stretch.*RefOuterRadius;
123
124 % Open files to save data into
125 fid1 = fopen(['OuterDiameter' num2str(Pdate{1}) '_' num2str(n) '.txt'],'w');
126 fid2 = fopen(['CrackLength' num2str(Pdate{1}) '_' num2str(n) '.txt'],'w');
127 fid3 = fopen(['StretchStack' num2str(Pdate{1}) '_' num2str(n) '.txt'],'w');
128 % fid4 = fopen(['TimeStack' num2str(Pdate{1}) '_' num2str(n) '.txt'],'w');
129 % Get size data for stacks
130 [row1,col1] = size(FinalStretch(:,1));
131 [row2,col2] = size(FinalCrack(:,1));
132 [row3,col3] = size(Stretch(:,1));
133 % [row4,col4] = size(ImageLoopNum(:,1));
134 % Formatting for fprintf function
```

```
135 z1 = repmat('%d\t',1,(col1-1));
136 z2 = repmat('%d\t',1,(col2-1));
137 z3 = repmat('%d\t',1,(col3-1));
138 % z4 = repmat('%d\t',1,(col4-1));
139
140 % Writes data into file and saves
141 fprintf(fid1,[z1,'%d\n'],FinalStretch(:,1)');
142 fprintf(fid2,[z2,'%d\n'],FinalCrack(:,1)');
143 fprintf(fid3,[z3,'%d\n'],Stretch(:,1)');
144 % fprintf(fid4,[z4,'%d\n'],ImageLoopNum(:,1)');
145
146 end
147
148
149 %------------------------------------------------------------------------
```

D.4 Least Square Determination of Viscoelastic Parameters

```
clear
clc
format long;

% Data for linear least squares
% Data is loaded from an excel spreadsheet
Creep   = xlsread('Creep 081217 Chandler 3 pH ver 2.xlsx','Creep 600 Pa (3 pH)','A03:A0473');
DTime   = xlsread('Creep 081217 Chandler 3 pH ver 2.xlsx','Creep 600 Pa (3 pH)','B3:B473');
% Determines size of array
[N X]   = size(Creep);
Temp    = ones(N,1);
% Creates A matrix in Ax=b for least squares approxiamtion
A       = [Temp,log(DTime)];
% Creates b vector in Ax=b for least squares approximation
b       = log(Creep);
% The matlab least squares algorithm.
F       = A\b;
% The viscoelastic parameters from J(t) = A0 t^n
A0      = exp(F(1,1))
n       = F(2,1)
```